

---

# A DATA-BASED COMPARATIVE REVIEW AND AI-DRIVEN SYMBOLIC MODEL FOR LONGITUDINAL DISPERSION COEFFICIENT IN NATURAL STREAMS

---

✉ **Yifeng Zhao**

Department of Environmental Science and Engineering  
Zhejiang University  
Hangzhou, CHN  
&  
School of Engineering  
Westlake University  
Hangzhou, CHN  
zhaoyifeng@westlake.edu.cn

✉ **Zicheng Liu**

School of Engineering  
Westlake University  
Hangzhou, CHN  
liuzicheng@westlake.edu.cn

✉ **Pei Zhang**

School of Engineering  
Westlake University  
Hangzhou, CHN  
zhangpei@westlake.edu.cn

✉ **S.A. Galindo-Torres\***

School of Engineering  
Westlake University  
Hangzhou, CHN  
s.torres@westlake.edu.cn

✉ **Stan Z. Li†**

School of Engineering  
Westlake University  
Hangzhou, CHN  
stan.zq.li@westlake.edu.cn

## ABSTRACT

A better understanding of contaminant spills in natural streams requires knowledge of Longitudinal Dispersion Coefficient (LDC). Various methods have been proposed for predictions of LDC. Those studies can be grouped into three types: analytical, statistical, and Machine Learning (ML) driven researches. However, a comprehensive evaluation of them is still lacking. In this paper, we first present an in-depth analysis of those methods and reveal some of their drawbacks. This is carried out on an extensive database composed of 660 samples of hydraulic and channel properties worldwide. The reliability and representativeness of the data are enhanced by deploying the Subset Selection of Maximum Dissimilarity (SSMD) for separation of subsets and the Inter Quartile Range (IQR) for removal of outliers. The analysis reveals the rank of those different methods as: ML-driven method > the statistical method > the analytical method. Where the '>' represents greater predictive performance. To establish an interpretable model for LDC prediction with higher performance, we design a novel interpretable regression method called evolutionary symbolic regression network (ESRN). It is a combination of genetic algorithms and neural networks. Strategies are introduced to avoid overfitting and explore more parameter combinations. Results show that the ESRN model distilled with a larger dataset and better processing strategies has superiorities over other existing symbolic models in performance and reliability. Also, a striking finding is that ESRN produced a simpler formula with a smaller number of parameters than the existing alternatives. Its simplicity allows us to connect this relation to the fundamental turbulent mixing process, illustrating this is the underlying physics behind the LDC in rivers. The proposed model is suitable for practical engineering problems and can provide convincing solutions for situations where the field test cannot be carried out, or limited field information can be obtained.

---

\*Co-corresponding author

†Co-corresponding author

**Keywords** Longitudinal dispersion coefficient · Symbolic regression · Evolutionary Symbolic Regression Network algorithm · Natural streams

## 1 Introduction

Natural streams play a pivotal role in the cycle of water resources on the earth. They have a strong impact on human water utilization processes, such as agriculture, ecology, cities, and industry. Meanwhile, they receive different kinds of contamination during these processes. Some of them, especially chemical and waste compounds, are crucial to the quality assessment of streams. In recent years, frequent contaminant spills have caused significant public attention. In Norilsk of Russia (2020), more than 135 square miles of the area have been contaminated due to an oil spill[1]. In Fukushima of Japan (2019) the report of the nuclear waste leak has caused great panic around the pacific rim[2]. In West Virginia of USA (2014), more than 300,000 people were affected by a toxic compound spill[3]. Among these cases, the pollution will spread throughout the ecosystem, not only to the lower algae animals but also to the human level. Recent studies have shown that the stream contamination is a potential cause of various diseases to both humans and other mammals[4, 5, 6]. Without an accurate tool to quantify this process, it is challenging to assess the quality of the stream and the overall pollution status, which makes it more time-consuming to fully solve this problem and restore the environment to its original state. On top of this, it is often challenging to determine the specific scope of impact with present techniques.

To control and reduce the damage of similar water pollution incidents, an effective method is to use simulation technology to evaluate the overall water status, which is faster and covers a broader range than the traditional sampling detection method. However, the existing simulation algorithms developed according to established theories have revealed mismatches through comparison of the sampling test method in several applications[7]. To improve accuracy, it is vital to obtain a deeper understanding of this phenomenon.

When scalars enter the stream, a 3-D process will be involved. In the early stage of the entrance, the advection will be dominant due to flow velocity for a short period of time. After the scalar is fully mixed, a balance between advection and diffusion will be reached. Then the longitudinal advection and dispersion start to reign. The general Advection Diffusion Equation (ADE, Eq. 1) can be used for further description.

$$\frac{\partial C}{\partial t} = \nabla \cdot (D_l \nabla C) - \nabla \cdot (UC) + R \quad (1)$$

Where C - the concentration; t - the time;  $D_l$  - the longitudinal dispersion coefficient; U - the flow velocity; R - the reaction term signaling either sources or sinks of the solute.

As for solutions to the ADE, both analytical and numerical methods have been developed in the past[8, 9, 10]. These studies showed that  $D_l$  is the most significant parameter for the accuracy of ADE solutions[11]. The field measurement of  $D_l$  can be costly and time-consuming. Therefore, many attempts have been made on the prediction of  $D_l$  with its wide range of influence variables. Major methods for prediction are the analytical, statistical, and the Machine Learning driven method. However, the present methods to obtain  $D_l$  cannot fully satisfy the need for practical engineering[5, 12, 13]. Those methods suffer from several disadvantages, such as weak prediction, poor generalization, and *black-box* nature (The property of algorithms and techniques that give no explicit explanation of working mechanisms).

To remedy this, a novel evolutionary symbolic regression network is proposed to distill predictive equations for  $D_l$  from extensive field data. The resulting  $D_l$  formula shows superiority in accuracy and generalization than previous researches. It also indicates the underlying physics behind the LDC is the turbulent mixing process.

The remainder of this paper is organized as follows: Section 2 is a detailed review of past research on the prediction of  $D_l$ . Section 3 consists of three parts: *Data exploratory and pre-process*, *Training and testing sets* and *Evaluation on previous studies*. *Data exploratory and pre-process* illustrates the strong data basis of this paper, a dataset of 1094 samples. Pre-processes, especially the removal of outliers with Inter Quartile Range (IQR), are also carried out in this part. *Training and testing sets* refers to the use of the Subset Selection of Maximum Dissimilarity (SSMD) to separate the dataset into the training set and testing set with the same distribution. *Evaluation on previous studies* presents a comparison between different models and methods for the prediction of  $D_l$ . Section 4 reveals the theory and design of the novel symbolic regression algorithm used in this study. In Section 5, the novel  $D_l$  prediction equation is presented. Multiple techniques are used to evaluate its performance and the result reveals its superiority over other research. Finally, Section 6 summarizes the contribution and indicates possible improvements for future studies.

Table 1: Summary of analytical model on  $D_l$ 

Seq	Author / Year	The formula	Application
1	Taylor / 1953	$D_l = \frac{(aU)^2}{48D_p}$	The laminar pipe flow
2	Taylor / 1953	$D_l = 10.06au_*$	The turbulent circular pipe flow
3	Elder / 1959	$D_l = \left(\frac{0.4041}{\kappa^3} + \frac{\kappa}{6}\right)dU^*$ or $D = 5.86dU^*$	The open channel flow
4	Fischer / 1968	$D_l = \int_0^w du' \int_0^y \frac{1}{\epsilon_t d} \int_0^y du' dy dy dy$	The open channel flow

\*  $D_l$  - the longitudinal dispersion coefficient;  $a$  - The radius of the pipe;  $D_p$  - The diffusion coefficient of particles;  $u_*$  - The shear velocity of circular pipe flow, equal to  $\left(\frac{gaS}{2}\right)^{0.5}$ , where  $S$  is the energy slope;  $U$  - The flow velocity;  $U^*$  - The shear velocity of natural streams, equal to  $(gRS)^{0.5}$ , where  $R$  is the hydraulic radius;  $w$  - the average channel width;  $d$  - the average channel depth;  $\kappa$  - the von Karman constant, approximately equal to 0.41;  $u'$  - the deviation of the velocity from the cross-sectional mean velocity;  $y$  - Cartesian coordinate in the lateral direction;  $\epsilon_t$  - the transverse turbulent diffusion coefficient.

## 2 Previous studies on the prediction of $D_l$

$D_l$  has many potential impact factors, such as stream properties, hydraulic conditions, and channel geometrics. According to turbulence properties of flow and simplification in flow-path parameters, it is found that the most important variables are: the average channel width -  $w$ , the average channel depth -  $d$ , the flow velocity -  $U$ , and the shear velocity -  $U^*$ [14, 15, 16, 17]. In this framework, many studies have been carried out. Studies on this topic can be divided into three categories: analytical, statistical, and the ML-driven method.

The analytical method combines mathematical principles and conceptual abstractions to obtain an approximate prediction. It is the first solution applied to this problem and several successful cases have already been achieved under ideal conditions, such as laminar flow in a pipe[18], turbulent circular flow in a pipe[19], and open channel flow[20, 21, 11]. Some of those studies are listed in Table 1.

Although those studies are still used in many engineering problems today, they suffer from several defects. A good example is that those prediction formulas are obtained under certain assumptions. The demand in detailed flow properties ( $D_p$ ,  $S$ ) and cross-sectional information ( $y$ ,  $\epsilon_t$ ) is also hard to satisfy. Besides, forms of some equations (Fischer/1978, Taylor / 1953 and Elder/1959) are overly complicated. These drawbacks restrict their application in more complex engineering problems.

To remedy those weakness, Fischer[11] applied statistical methods on the research of  $D_l$ . By introducing four macro-variables:  $d$ ,  $w$ ,  $U$  and  $U^*$ , the prediction equation is simplified and the  $D_l$  is connected to its geometric and hydrologic variables (Eq. 2).

$$\frac{D_l}{dU^*} = 0.011 \left(\frac{w}{d}\right)^2 \left(\frac{U}{U^*}\right)^2 \quad (2)$$

After that, through use of various statistical methods and expansion of the  $D_l$  dataset, a series of studies are carried out (Table 2). Utilizing the similarity between the 1D flow equation and 1D dispersion equation, McQuivey and Keefer[22] developed a simplified equation for  $D_l$  problem with Froude number ( $Fr$ ) less than 0.5, where the Froude Number is defined as:

$$Fr = \frac{U}{\sqrt{gL}} \quad (3)$$

where  $g$  - the local external field;  $L$  - the characteristic length.

Liu et al.[23] modified Fischer's equation (Eq. 2) to a form which contains a gradient of lateral velocity. Through fitting, a highly simplified formula was proposed; Dimensional analysis was applied to this problem by Seo and Cheong for the first time[24]. The one-step Huber method, a famous nonlinear multi-regression method was then utilized on 59 field datasets to enhance the previous research; Koussis and Rodríguez-Mirasol applied Von Karman defect law to the original theory and equations formulated by Fischer(Eq. 2) and a modified equation was developed[25]; A theoretical approximation to generate a new equation based on Fischer work was made by Deng et al., and a more detailed expression of the channel depth, the flow velocity, and the local transverse mixing coefficient was proposed[26]; Through the expansion of dataset, Kashfipour and Falconer[27], Zeng and Huai[28] both presented improved  $D_l$  prediction formulas. Disley et al. incorporated the Froude number as a third key parameter other than  $w/d$  and  $U/U^*$ .

Table 2: Summary of statistical model on  $D_l$ 

Seq	Author / Year	The formula	Application
5	Fischer / 1979	$\frac{D_l}{dU^*} = 0.011(\frac{w}{d})^2(\frac{U}{U^*})^2$	Connect $D_l$ with its macro-variables with statistical methods for the first time
6	McQuivey and Keefer / 1975	$\frac{D_l}{dU^*} = 0.058(\frac{U}{SU^*})$	For Froude number less than 0.5
7	Liu et al. / 1977	$\frac{D_l}{dU^*} = 0.18(\frac{w}{d})^2(\frac{U}{U^*})^{0.5}$	Consider lateral velocity gradient
8	Seo and Cheong / 1998	$\frac{D_l}{dU^*} = 5.915(\frac{w}{d})^{0.62}(\frac{U}{U^*})^{1.428}$	Apply von Karmen defect law
9	Koussis and Rodríguez-Mirasol / 1998	$\frac{D_l}{dU^*} = 0.6(\frac{w}{d})^2$	Apply dimensional analysis
10	Deng et al. / 2001	$\frac{D_l}{dU^*} = (\frac{0.15}{8\epsilon})(\frac{w}{d})^{1.67}(\frac{U}{U^*})^2$	Introduce a new variable with detailed theoretical analysis
11	Kashefipour and Falconer / 2002	$\frac{w}{d} > 50, \frac{D_l}{dU^*} = 10.612(\frac{U}{U^*})^2$ $\frac{w}{d} \leq 50, \frac{D_l}{dU^*} = (7.428 + 1.775(\frac{w}{d})^{0.62})(\frac{U}{U^*})^{0.572}(\frac{U}{U^*})^2$	Propose a segmented symbolic equation
12	Zeng and Huai / 2014	$\frac{D_l}{dU^*} = 5.4(\frac{w}{d})^{0.7}(\frac{U}{U^*})^{1.13}$	Provide validation on trapezoidal artificial channels
13	Disley et al. / 2014	$\frac{D_l}{dU^*} = 3.563(\frac{U}{(gd)^{0.5}})^{-0.4117}(\frac{w}{d})^{0.6776}(\frac{U}{U^*})^{1.0132}$	Introduce a new variable into the formula

\*  $D_l$  - the longitudinal dispersion coefficient;  $w$  - the channel width;  $d$  - the channel depth;  $U$  - The flow velocity;  $U^*$  - The shear velocity;  $S$  - the energy slope;  $\epsilon$  - equal to  $0.145 + (\frac{w}{d})^{1.38}(\frac{U}{U^*})$ ;  $g$  - the acceleration of gravity.

This new combination achieved better results in the testing[29]. Those studies grasped the essence of the  $D_l$  prediction, a regression problem. More simple and practical results have been obtained with the use of different statistical regression methods and introduce of new variables.

However, inconsistency has been found between predictions of those statistical models and experimental results. The performance of those equations could vary widely under the same stream and geometric conditions[12, 7]. That is because those models are basically regressions of their own training datasets. But those methods are not capable of modeling this highly nonlinear phenomenon with only hundreds of samples. Besides, the lack of proper data pre-processing and data scarcity introduce uncertainty into those models. These defects are the main reason for this inconsistency[7]. For a more precise prediction, a modeling method with better general applicability for  $D_l$  and improvement on data are required.

The rise of ML-driven methods in related research provides a possible solution. Machine learning techniques have powerful regression ability, even on biased data. Taking neural networks(NN) for example, studies show that a two-layer NN can represent any underlying distribution in the data[30, 31, 32]. Moreover, the regression ability of those methods is not only limited to interpolation but also extrapolation. Its application potential has been verified in many scientific and engineering applications[33, 34, 35]. On the prediction of  $D_l$ , several ML-driven studies have revealed apparent superiority over other methods, especially in accuracy and precision. Based on whether symbolic equations will be proposed, the used ML method can be further divided into implicit and explicit methods.

Implicit ML-driven methods refer to various kinds of machine learning techniques which cannot give clear and simple symbolic expressions of models. Representative methods are neural network (NN) and support vector machine (SVM). Those methods are generally used as *black boxes* in applications. However, It doesn't mean that such methods cannot provide symbolic equations for their calculation process. They are used as black boxes mainly because their symbolic equations are too complicated to represent and understand. On the contrary, the explicit ML-driven method can give a much simpler mathematical model, which is easy to use, interpret and give physical meaning, increasing both our predictive power and the insight behind the complex phenomenon.

Implicit ML-driven methods are used earlier on the prediction of  $D_l$ . NNs with different designs were used to forecast the dispersion process by Tayfur and Singh[36], Topark and Cigizoglu[37], and Noori et al.[12]; The performance of the adaptive neuro-fuzzy inference system(ANFIS) was examined by Noori et al.[38] and Riahi-Madvar et al.[39]; Azamathulla and Wu[40] developed a support vector machine(SVM) approach for this problem; Hybrid genetic expression programming(GEP) was applied on this topic by Alizadeh et al. [16] and four different metaheuristic algorithms were evaluated; The advantages and disadvantages of NN and GEP were discussed by Seifi and Riahi-Madvar [41]; Ghiasi et al.[42] carried out a successful application of the granular computing (GRC) method as well as sensitivity analysis. Results show that the parameter,  $\frac{w}{d}$  matters most on the output in all models. Among them, NN is the most widely used method[36, 37, 12, 16, 41, 42]. All of those machine learning techniques achieve excellent predictions on  $D_l$ . But their black-box nature limits further understandings of underlying physics and bring uncertainty into field application.

To remedy the black-box attribute, several explicit ML-driven methods dedicated to finding symbolic formulas have been used. Sahay and Dutta[43] reported an application of a genetic algorithm for the regression of symbolic equations of  $D_l$  formulas. A concise equation was regressed directly from data; Etemad-Shahidi and Taghipour[44] combined

Table 3: Summary of explicit ML-driven formulas on  $D_l$ 

seq	Author / Year	The formula	Application
14	Sahay and Dutta / 2009	$\frac{D_l}{dU^*} = 2\left(\frac{w}{d}\right)^{0.96}\left(\frac{U}{U^*}\right)^{1.25}$	Genetic algorithm
15	Li et al. / 2013	$\frac{D_l}{dU^*} = 2.2820\left(\frac{w}{d}\right)^{0.7613}\left(\frac{U}{U^*}\right)^{1.4713}$	Differential evolution algorithm
16, 17	Scatter and Gharabaghi / 2015	$\frac{D_l}{dU^*} = a\left(\frac{w}{d}\right)^b\left(\frac{U}{U^*}\right)^c$ <i>Model</i> <sub>17</sub> : $a = 2.9 \times 4.6\sqrt{F_r}$ , $b = 0.5 - F_r$ , $c = 1 + \sqrt{F_r}$ , $d = -0.5$ <i>Model</i> <sub>18</sub> : $a = 8.45$ , $b = 0.5 - 0.514F_r^{0.516} + \frac{U}{U^*}0.42\sqrt{F_r}$ , $c = 1.65$ , $d = 0$ $F_r = \frac{U}{\sqrt{gd}}$	Genetic algorithm
18	Wang and Huai / 2016	$\frac{D_l}{dU^*} = 17.648\left(\frac{w}{d}\right)^{0.3619}\left(\frac{U}{U^*}\right)^{1.16}$	Genetic algorithm
19	Wang and Huai / 2017	$\frac{D_l}{dU^*} = (0.718 + 47.9\frac{d}{w})\frac{U}{w}$	Genetic algorithm
20	Alizadeh et al. / 2017	$\frac{w}{d} > 28$ , $\frac{D_l}{dU^*} = 9.931\left(\frac{w}{d}\right)^{0.187}\left(\frac{U}{U^*}\right)^{1.802}$ $\frac{w}{d} \leq 28$ , $\frac{D_l}{dU^*} = 5.319\left(\frac{w}{d}\right)^{1.206}\left(\frac{U}{U^*}\right)^{0.075}$	Optimization algorithm
21	Riahi-Madvar et al. / 2019	$\frac{D_l}{dU^*} = 33.99\left(\frac{w}{d}\right)^{0.5} + 8.497\frac{w}{d}\left(\frac{U^*}{U}\right)^2 + \frac{8.497wU^*}{dU}$ $16.99\frac{wU^*}{dU} + \frac{0.000486\left(\frac{w}{d}\right)^{0.5} - 0.00021}{d^{1.5}(U^*)^4}w^{1.6}U^4 + 0.01478$	Optimization algorithm
22,23	Memarzadeh, R., et al. / 2020	<i>Model</i> <sub>22</sub> : $\frac{w}{d} > 27$ , $\frac{D_l}{dU^*} = (0.35 + 8.7\left(\frac{d}{w}\right))(6.4 + 8\left(\frac{w}{d}\right))\left(\frac{U}{U^*}\right)^{0.5}$ $\frac{w}{d} \leq 27$ , $\frac{D_l}{dU^*} = 0.2694\left(\frac{w}{d}\right)^{2.2456}$ <i>Model</i> <sub>23</sub> : For all data, $\frac{D_l}{dU^*} = 4.5\left(\frac{w}{d}\right)\left(\frac{U}{U^*}\right)^{0.5}$	Optimization algorithm
24,25	Riahi-Madvar et al. / 2020	<i>Model</i> <sub>24</sub> : $a = 1 + e^{-0.02w+0.39d+3.52U+11.37U^*-3.72}$ $b = 1 + e^{0.02w-0.48d+0.69U+11.37U^*+2.37}$ $c = 1 + e^{0.02w+0.87d-3.52U-2.04U^*-4.48}$ $d = 1 + e^{0.03w+1.6d+3.52U-4.49U^*-11.6}$ $D_l = \frac{-124.74}{a} + \frac{374.99}{b} - \frac{517.15}{c} - \frac{636.76}{d} + 227.59$ <i>Model</i> <sub>25</sub> : $a = 1 + e^{0.04w-0.62d-2.71U+23.26U^*-9.21}$ $b = 1 + e^{-0.023w+1.31d+0.54U+10.18U^*+1.91}$ $c = 1 + e^{0.021w+0.11d+2.04U-3.60U^*-7.25}$ $d = 1 + e^{0.01w+1.07d+2.14U+0.335U^*-7.20}$ $e = 1 + e^{-0.01w-0.24d+7.94U+1.49U^*+2.33}$ $D_l = \frac{471.22}{a} + \frac{315.96}{b} - \frac{306.77}{c} - \frac{818.23}{d} - \frac{583.71}{e} + 227.59$	Neural network

\*  $D_l$  - the longitudinal dispersion coefficient;  $w$  - the channel width;  $d$  - the channel depth;  $U$  - The flow velocity;  $U^*$  - The shear velocity;  $F_r$  - Froude number.

the M5 model tree and 149 data samples to propose a novel symbolic result. However, the performance of this symbolic model was unsatisfying; By minimizing the sum-square error, a differential evolution(DE) algorithm was successfully applied to this problem by Li et al.[45]. 65 samples from 29 rivers in the USA were analyzed; Satter and Gharabaghi developed two gene expression models of  $D_l$  and its various hydraulic variables, including the Froude number, aspect ratio, and the bed material roughness[46]. A parametric analysis is performed for further verification; Wang et al. proposed a more concise and accurate canonical equation form by distilling the physical meaning of dispersion[47]. Based on the novel combination, genetic programming without pre-specified correlations combined with a theoretical method was used to fit a physically sound explicit predictor[47, 48]; A multi-objective particle swarm (PSO) optimization technique was applied to drive a novel equation to estimate the D by Alizadeh et al.[16]. Extensive field data, including various hydraulic and geometric parameters, were utilized; On the same 503-sample dataset, Riahi-Madvar et al. [49] and Memarzadeh, R., et al. [13] combined optimization algorithms with the Subset Selection of Maximum Dissimilarity(SSMD), a division method for the training set and testing set. Results show the model of Memarzadeh, R., et al. [13] has better accuracy; Riahi-Madvar et al.[50] implemented the prediction equation of  $D_l$  into the NN and utilized the powerful regression capabilities of NN to fit parameters. However, the equation obtained was overly complicated. Explicit formulas from the above studies are shown in Table 3. As can be seen, the formulas are complicated, with little physical meaning. It is reasonable to suspect that they are subject of overfitting.

Nevertheless, those explicit ML-driven methods are weaker than implicit methods in performance[39, 43, 46, 13] Detailed Comparisons can be found in Section 3.3. This is generally caused by two factors: data scarcity and algorithm defects. Most of the studies use only dozens of data, which is far from enough to predict this highly nonlinear process. More data samples are needed.

Apart from the data problem, those algorithms suffer from several defects. Most of the algorithms are doing fitting for parameters of a fixed formula form(Eq. 4).

$$D_l = p_1 \left( \frac{w}{d} \right)^{p_2} \left( \frac{U}{U^*} \right)^{p_3} \quad (4)$$

where  $p_1$ ,  $p_2$  and  $p_3$  are different parameters.

Few studies have explored other possible combinations of functional forms and parameters. Some of them do try different symbolic equation forms, but mainly by test and trail[46, 50] which is inefficient and incomplete. Besides, the main drawback of those algorithms is extrapolation ability. These models perform poorly under new data samples (See details in Section 3.3). Those factors make the present explicit formulae unsuitable to satisfy the application demand on the prediction of  $D_l$ . Due to these reasons, there is a pressing need for an improved symbolic regression framework.

To propose a high-performance, interpretable  $D_l$  prediction equation, the above two obstacles need to be tackled correspondingly. For data scarcity, a large and convincing dataset is needed. For algorithm defects, a novel scheme is required. On one hand, It should be able to explore more possible formula forms exhaustively and find the more accurate combination. On the other hand, it needs to have strong regression ability, which can achieve better results in interpolation and extrapolation. Details on solutions for these two obstacles will be discussed in Section 3 and Section 4 separately.

### 3 Data

#### 3.1 Data exploratory and pre-process

Data is pivotal to the development of governing equations. Generally, samples and features of the used dataset will determine the upper limit of the predictive model. Different regression methods are just struggling to reach this limit[51]. Therefore, it is necessary to do some analysis and processing on the data foundation.

In this study, a dataset of 1094 samples, which contain measured  $D_l$  and its influence variables ( $w$ ,  $d$ ,  $U$ , and  $U^*$ ) in various streams all over the world, is collected from published works[24, 15, 52, 53, 54, 55, 56, 57, 58].

Since these samples are collected from different streams globally, it is helpful to have preliminary knowledge of the patterns behind them. According to the adversarial validation test(Presented in supplementary material, Section S1), there are three groups of samples, which demonstrates the data diversity.

After deleting null values and duplication, a dataset of 721 samples is obtained. But there are some outliers in the data(Fig. 1). Many previous studies have mentioned the influence of extreme values[17, 59, 52]. This effect is usually solved through removal by tests and trails, which has low efficiency and lack of theoretical support. Such extreme values are highly possible to be outliers caused by variability in measurement or experimental errors[60]. The existing of them can bring uncertainty into the result. But few previous studies conducted reasonable outlier removal. To remove those errors, the Inter Quartile Range(IQR) is introduced. IQR is a measure of statistical discrete degree (Eq. 5). It can reveal the dispersion of variables in the dataset, which is often used in removal of the outlier.

$$IQR = Q3 - Q1 \quad (5)$$

where for a  $2n$  or  $2n + 1$  set of samples,  $Q3$  = the median of the  $n$  largest samples;  $Q1$  = the median of the  $n$  smallest samples.

Samples out of  $[Q1 - 1.5 * IQR, Q3 + 1.5 * IQR]$  are usually considered as outliers. After selection by IQR, a dataset of 660 samples is obtained (Fig. 1).

To have a basic understanding of the data distribution in the processed dataset, the kernel density plot (KDP, Fig. 2) and the pair plot (Fig. 3) are carried out. KDE aims to reveal the underlying distribution density of samples with the Gaussian kernel[?]. It shows that all parameters in this dataset have a normal distribution, which satisfies the Central Limit Theorem. This will ensure the extraction formula to be universal and robust[60]. The pairplot can reveal the pairwise relationships between every two involved parameters in a group. As shown in Fig. 3, the relationship between the input parameters ( $w$ ,  $d$ ,  $U$  and  $U^*$ ) and the output parameter ( $D_l$ ) is not linear and hard to get useful information.

Therefore, the Spearman Correlation Coefficient (SCC) is calculated. SCC is a statistical measure of the monotonic correlation between variables[?]. It is less affected by outliers than Pearson Correlation Coefficient, which is used in many studies[24, 17, 14] to reveal parameter relationships. Fig. 4 is the SCC plot of input and output parameters, in which the number stands for the SCC value between the two involved parameters.

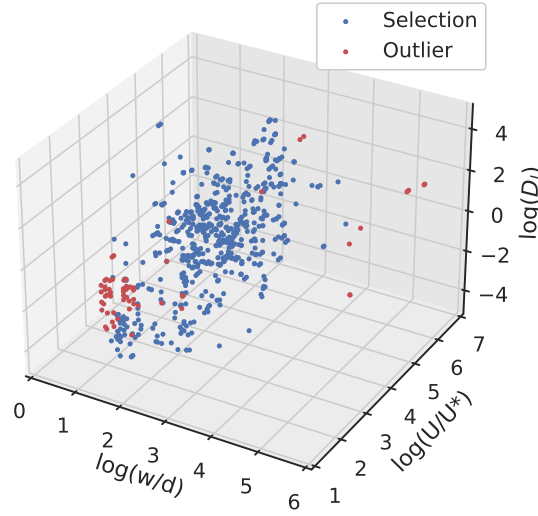


Figure 1: The visualization of selections and outliers

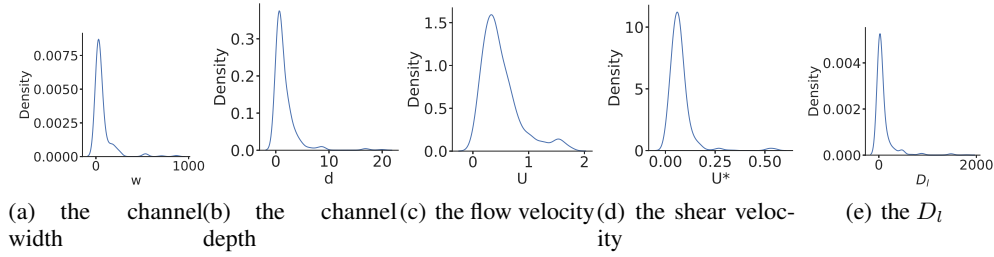


Figure 2: The kernel density plot of four input parameters

The Figure shows that channel geometries have stronger relationships with  $D_l$  than stream properties ( $D_l - d=0.56$ ,  $D_l - w = 0.71 > D_l - U = 0.38$ ,  $D_l - U_s=0.29$ ). In channel geometries, the channel width,  $w$  has the strongest influence, which means  $w$  is the most important variable to  $D_l$ . It is worth noting that stream properties have a weak relationship with channel geometrics, especially  $U_s$  ( $U_s - w=0.07$ ,  $U_s - d=0.09$ ). Besides, channel geometrics and streams properties both have a strong internal correlation ( $w - d=0.78$ ,  $U - U^*=0.50$ ), verifying the rationality of data.

The statistical information on this dataset is shown in Table 4. Selected metrics include: number (Num), minimum (Min), median (Med), maximum (Max), interquartile range (IQR), standard deviation (std), variance (Var), kurtosis (Kurt), median absolute deviation (MSD), and skewness(Skew).

Table 4: The statistical analysis of the data after cleaning

Parameter	Num	Min	Med	Max	IQR	std	Var	Kurt	MAD	Skew
d	660	0.03	0.88	19.94	1.61	2.31	5.33	25.72	0.53	4.39
w	660	0.20	34.95	867	47.75	113.06	12783	21.95	19.95	4.26
U	660	0.03	0.41	1.74	0.36	0.35	0.12	2.26	0.18	1.52
U*	660	0.002	0.06	0.553	0.040	0.065	0.004	29.009	0.020	4.691
D	660	0.01	25.90	1798.60	62.25	205.59	42265	26.31	20.55	4.63

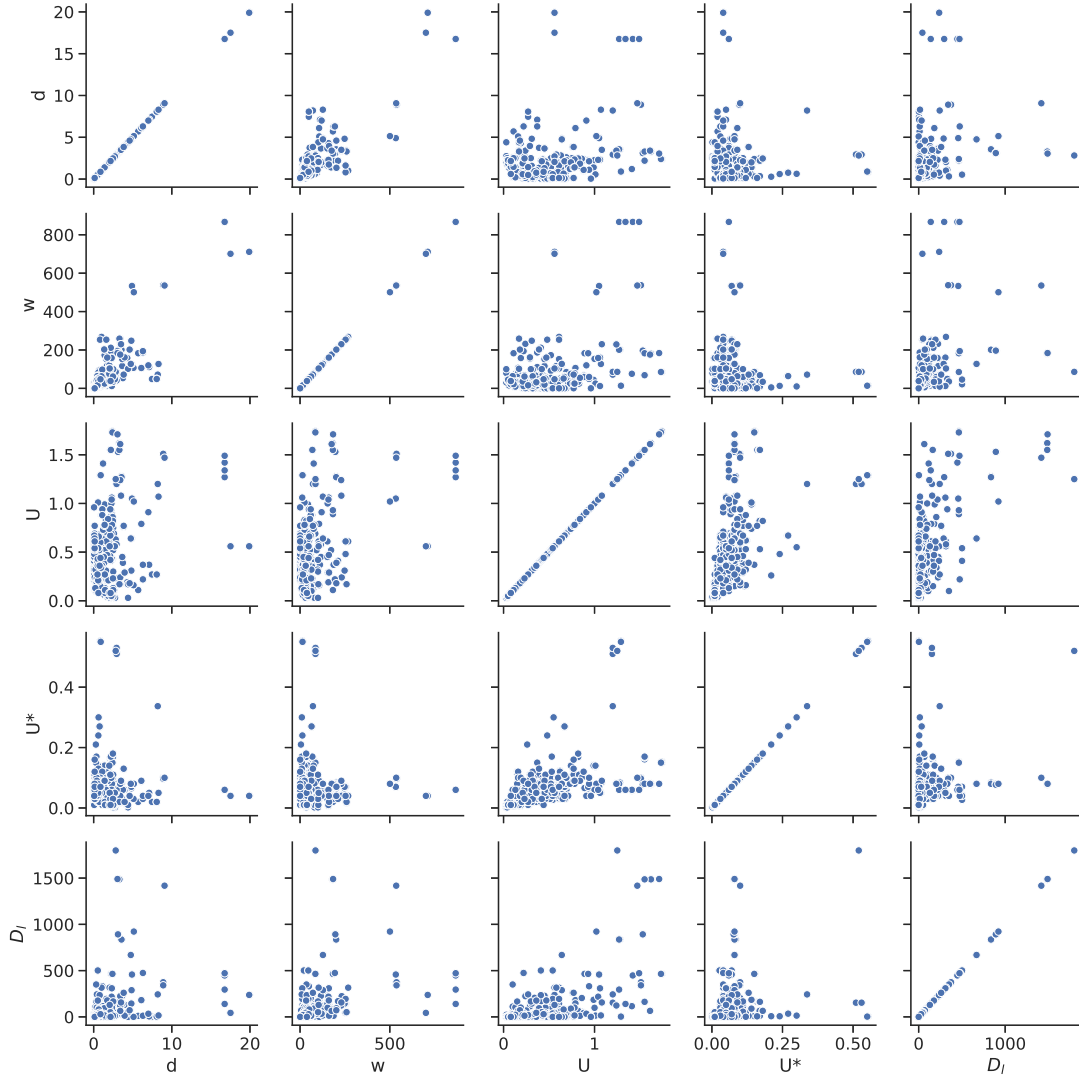


Figure 3: The pairplot of the data after cleaning

### 3.2 Training and testing sets

For the regression of  $D_l$  equation, 462 samples (about 70% of the overall dataset) will be used for development and the remaining 198 samples (30% of the overall dataset) will be used for testing.

Testing set selection is essential to model development. It can both direct the adjustment of the model's super-parameters and assess the performance of the model under new data[61, 62]. The dataset used in this paper is much larger (at least 20%) than other related research. And due to the diversity of samples and the satisfaction of Central Limit Theorem, the dataset also has advantages in comprehensiveness. Newly measured data is highly probable to locate within the distribution and range of our dataset. However, a randomly divided test set is highly possible to have distribution different from the original dataset, which will make the developed model biased and the testing result doubtful. To generate reliable subsets, the Subset Selection of Maximum Dissimilarity (SSMD) algorithm is implemented.

SSMD is a selection strategy, which dedicates to filter out samples with the greatest similarity to the original dataset[63]. The details of this algorithm are presented in supplementary material, Section S2.

Fig. 5 is the visualization of training and testing sets separated by SSMD. The statistics of parameters in the training and testing dataset are given in Table 5. Results show that all parameters have almost the same distribution and



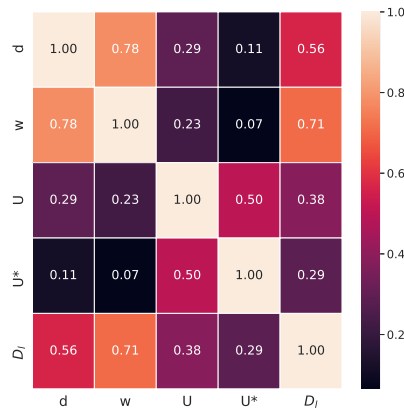


Figure 4: The SCC plot of  $w$ ,  $d$ ,  $U$  and  $U^*$

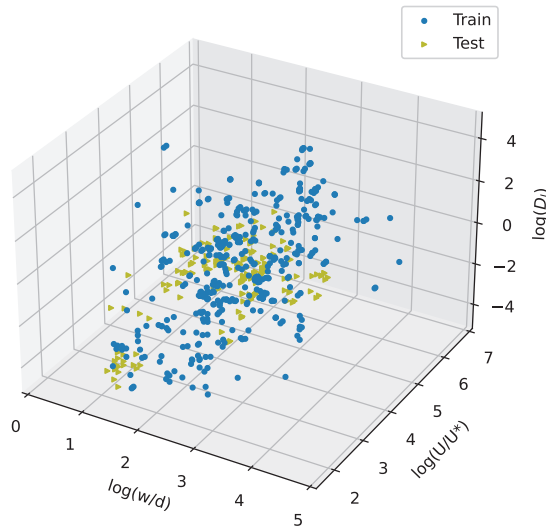


Figure 5: The visualization of training and testing sets separated by SSMD

characteristics in both sets. It is worth mentioning that the ranges of parameters are not precisely the same in training and testing sets. Actually, the training-set range contains the testing-set range and those testing samples are evenly scattered in the region of the training set. This can avoid the risk of overfitting and guarantee the robustness of the developed model[64].

### 3.3 Evaluation on previous studies

Although extensive research has been carried out on  $D_l$ , there is limited awareness of the need for objective and comprehensive comparison of these works. This makes the understanding of connections among those research results unclear. For example, it is hard to judge which type of method is more suitable for the prediction of  $D_l$  based on separate studies. The main obstacle is the lack of an appropriate, adequate database. However, datasets used in previous research are not the same. Most of the datasets are small, only dozens or hundreds of samples, which lack representativeness. The missing of proper data cleaning can easily make the previous evaluation biased. Defects in the database make the simple comparison of evaluation indexes in different studies meaningless. The uncertainty in model training also creates difficulties. In application of those methods, the selection of hyperparameters is often done by test and trail.

Table 5: The statistical properties of training set and testing set

Subset	Parameter	Num.	Min	Max	IQR	std	Var	Kurt	MAD	Skew
Training set	d	462	0.03	19.94	1.96	2.65	7.04	18.34	0.91	3.73
	w	462	0.20	867	73.10	130.87	17128.09	14.98	25.16	3.56
	U	462	0.03	1.74	0.52	0.41	0.17	0.59	0.23	1.13
	U*	462	0.002	0.553	0.041	0.077	0.006	20.430	0.023	4.044
	$D_l$	462	0.01	1798.60	121.40	239.74	57477.19	17.96	27.45	3.87
Testing set	d	198	0.08	2.49	0.51	0.51	0.26	2.84	0.27	1.43
	w	198	0.40	97.54	25.83	21.60	466.53	1.04	11.23	0.99
	U	198	0.28	0.63	0.13	0.09	0.01	0.52	0.06	0.56
	U*	198	0.030	0.130	0.020	0.028	0.001	0.127	0.010	0.497
	$D_l$	198	0.01	234.69	26.46	39.88	1590.58	6.93	13.65	2.47

Table 6: The evaluation of statistical models

Seq	RMSE	WMAPE	R2	DR				Accuracy (-0.3<dr<0.3)
				dr ≤ -0.3	-0.3 < dr ≤ 0	0 < dr ≤ 0.3	dr > 0.3	
Model 5	1758.58	4.81	-72.28	0.24	0.13	0.18	0.45	30.91
Model 7	378.45	1.40	-2.39	0.18	0.18	0.28	0.35	46.82
Model 8	572.65	1.57	-6.77	0.13	0.14	0.28	0.45	42.12
Model 9	362.96	1.49	-2.12	0.12	0.15	0.30	0.43	44.70
Model 10	423.51	1.23	-3.25	0.15	0.16	0.27	0.43	42.42
Model 11	491.58	1.29	-4.73	0.22	0.28	0.16	0.34	43.79
Model 12	291.60	0.96	-1.01	0.19	0.22	0.25	0.35	46.52
Model 13	309.66	1.01	-1.27	0.12	0.25	0.24	0.38	49.55

This could cause results obtained with the same method distinctly, which will make it very hard to carry out proper performance comparison.

To carry out a reliable comparison, these two problems need to be solved. The first problem can be easily tackled with the development of datasets in the previous two sections. The dataset in this paper is fairly large and cleaned carefully. It can fully reflect the potential performance of models in real life. As for the second problem, it will be solved through a general assessment. SVM, ANFIS and NN are the most commonly used approaches in implicit ML-driven studies. The main differences between similar studies in each approach are the hyperparameters of the model and used datasets. In our evaluation, the average performance is more concerned than the specific performance limits. Those different methods will be each implemented multiple times with random hyperparameters to get an average performance score. Then average scores of those models will be recorded to display their prediction abilities.

The objectives in this evaluation are: statistical prediction formulas (9 equations, Table 2), explicit ML-driven prediction formulas (9 equations, Table 3) and implicit ML-driven prediction models (SVM, ANFIS, NN, and ElasticNet). An internal evaluation of each method will be first made. Then the best two models in each method will be selected for further external comparison.

The evaluation metrics used are Root Mean Squared Error (RMSE), Mean Absolute Percentage Error (WMAPE), R-Square ( $R^2$ ) and Discrepancy Ratio (DR). See definitions of these metrics in supplementary material, Section S3.

The evaluation result of statistical models is illustrated in Table 6 and the Taylor diagram in Fig. 6 (Model 6 is not included due to the paucity of data on the energy slope). The result shows that RMSE values are quite high. Most WMAPE values are over 1.00 and  $R^2$  negative. The average accuracy of prediction is lower than 40%. The best two models in the statistical method are Zeng and Huai / 2014 (Model 8 in Fig. 6) and Disley et al. / 2014 (Model 9 in Fig. 6). All these metrics signal that the extrapolation ability of statistical models is poor. This is mainly because the complexity of the  $D_l$  problem has already surpassed the regression-ability limit of the statistical method.

Compared with statistical methods, explicit ML-driven methods achieve much better results. Due to stronger regression ability, all indexes of those studies are significantly improved (Table 7 and Fig. 7). The best model (Memarzadeh R., et al. / 2020, model 9 in Fig. 7) achieves R2 of 0.22 and prediction accuracy of 55%. The RMSE and WMAPE values decrease to 181.02 and 0.72. This shows that the prediction deviation is in a reasonable range. The assessment result shows that the explicit ML-driven method has better generalization ability than the statistical method. It can learn more patterns from samples and function more precisely in extrapolation prediction. The best two models in this branch are model 9 and 10 of Memarzadeh R., et al. / 2020. It is worth noting that the results of model 11 and model 12 are very poor. After verification, they are developed by combining the optimization algorithm and NN on a small data set (71

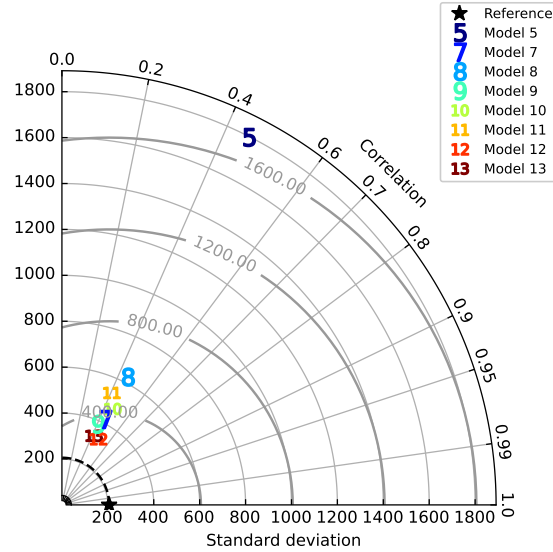


Figure 6: The Taylor diagram of statistical models

Model 5 - Fischer / 1975; Model 7 - Liu et al. / 1977; Model 8 - Seo and Cheong / 1998; Model 9 - Koussis and Rodr´ıguez-Mirasol / 1998; Model 10 - Deng et al. / 2001; Model 11 - Kashefipour and Falconer / 2002; Model 12 Zeng and Huai / 2014; Model 13 - Disley et al. / 2014.

Table 7: The evaluation of explicit ML-driven models

Seq	RMSE	WMAPE	R2	DR				Accuracy (-0.3<dr<0.3)
				dr ≤ -0.3	-0.3 < dr ≤ 0	0 < dr ≤ 0.3	dr > 0.3	
Model 14	439.56	1.28	-3.58	0.15	0.19	0.23	0.43	41.97
Model 15	434.98	1.21	-3.48	0.19	0.20	0.24	0.37	44.24
Model 16	408.89	1.18	-2.96	0.13	0.22	0.28	0.37	49.85
Model 17	499.63	1.32	-4.92	0.09	0.26	0.25	0.41	50.30
Model 18	274.09	0.94	-0.78	0.19	0.21	0.26	0.33	47.27
Model 19	217.01	0.84	-0.12	0.21	0.25	0.22	0.32	46.97
Model 20	521.13	1.25	-5.44	0.23	0.26	0.26	0.25	51.82
Model 21	1429.85	3.31	-47.45	0.17	0.20	0.24	0.39	43.48
Model 22	181.02	0.72	0.22	0.27	0.30	0.25	0.18	55.45
Model 23	183.13	0.74	0.21	0.22	0.28	0.21	0.29	49.09
Model 24	1010.22	10.35	-23.18	0.07	0.01	0.02	0.91	2.73
Model 25	906.64	9.45	-18.48	0.03	0.03	0.03	0.91	6.21

samples from [36]).  $R^2$  values in paper of Riahi-madvar[50] are 0.94 and 0.81 for training and testing sets, which are very high. This poor assessment result reveals that these two models suffer from critical over-fitting problem[65, 66]. The prediction result from these two models is biased towards the training dataset, which makes them lack applicable values. Therefore, model 11 and model 12 are not included in the visualization.

The result of implicit ML-driven methods is very satisfying(Table 8 and Fig. 8). The best model is the support vector machine (SVM, model 29 in Fig. 8). The  $R^2$  is about 0.36 and prediction accuracy over 60%, which indicate SVM has very high practical worth. However, NN and ANFIS, which should have stronger regression ability, underperform than SVM and ElasticNet. After analysis, this is mainly due to two reasons. Firstly, Network design of NN and ANFIS has very strong randomness[67]. There are no rules or modes for development at present and hyperparameters are usually selected by test and trial. This makes the model performance fluctuate in a certain range. It is possible to find a better model through costly hyperparameter selection. But as mentioned before, the average performance is the core of this section. A well-tuned NN or ANFIS model can only show that model is better but not the method. Secondly, stronger regression ability does not mean a superior model. Although detailed data cleaning is carried out, there are still some noises in samples. It can be inferred that NN tried to learn from those noises. In small dataset, NN can learn those noises very well[50] and then be prone to overfitting. Quite satisfying results can be obtained. However, samples from

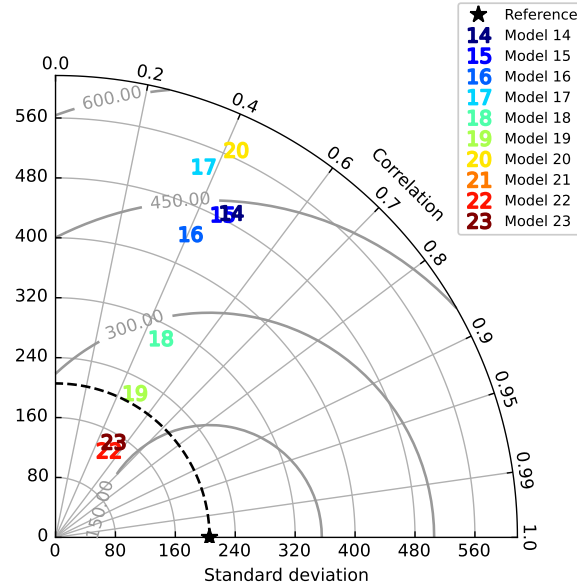


Figure 7: The Taylor diagram of the explicit ML-driven models where Model 14 - Sahay and Dutta / 2009; Model 15 - Li et al. / 2013; Model 16, 17 - Scatter and Gharabaghi / 2015; Model 18 - Wang and Huai / 2016; Model 19 - Wang and Huai / 2017; Model 20 - Alizadeh et al. / 2017; Model 21 - Riahi-Madvar / 2019; Model 22, 23 - Memarzadeh R., et al. / 2020; Model 24, 25 - Riahi-Madvar et al. / 2020.

Table 8: The evaluation of implicit ML-driven models

Seq	RMSE	WMAPE	R2	DR				Accuracy (-0.3<dr<0.3)
				$dr \leq -0.3$	$-0.3 < dr < 0$	$0 < dr < 0.3$	$dr \geq 0.3$	
Model 1	180.18	0.79	0.10	0.10	0.32	0.20	0.38	52.02
Model 2	199.30	0.76	0.13	0.16	0.10	0.20	0.54	53.55
Model 3	101.27	0.42	0.47	0.21	0.38	0.22	0.20	59.60
Model 4	59.50	0.32	0.51	0.14	0.34	0.26	0.26	68.80

different experiments will have different error distributions. When they come together, NN will try to learn all these errors, which causes the final result to be unsatisfying.

Through visualizing the best two models of each method (Fig. 9), the rank of three regression techniques is: Implicit ML-driven methods > Explicit ML-driven methods > statistical methods. Among them, statistical methods have limited extrapolation ability and implicit ML-driven methods suffer from their black-box nature, which make the Explicit ML-driven method to be the most proper solution to gain a fair compromise between predictability and understanding on this phenomenon. Optimization algorithms are popular methods in this field. But the regression problem is not a good topic for them [68, 69, 70]. Besides, there is still some performance distance between explicit ML-driven methods and implicit ML-driven methods (Fig. 9), which indicates room for improvement in explicit ML-driven methods.

It is interesting to note that the evaluation result of those models is much lower than the value reported in their papers. A common reason for all cases is the size effect of the training dataset. By plotting 100 prediction values point to point randomly (Fig. 10), it can be found that the main error sources are some extreme predictions. In the development of those models, the lack of outlier-cleaning and subset selection is common. Besides, the used datasets are usually small, only dozens of hundreds of samples, which can easily lead to a biased result. In the general form of  $D_l$  models (Eq. 4),  $d$  and  $U^*$  are divisible items (They appear in fraction denominators explicitly). With many small values in  $d$  and  $U^*$ , those biased models can generate huge predictive errors due to numerical singularities and deteriorate the model performance significantly.

However, this does not mean a larger dataset is inappropriate. A large dataset can bring advantages in both establishment and evaluation of the model. A larger dataset can also enable the model to discover more and better patterns, which guarantees the model to have a proper generalization ability. Taking models in [13] as examples, an explicit prediction

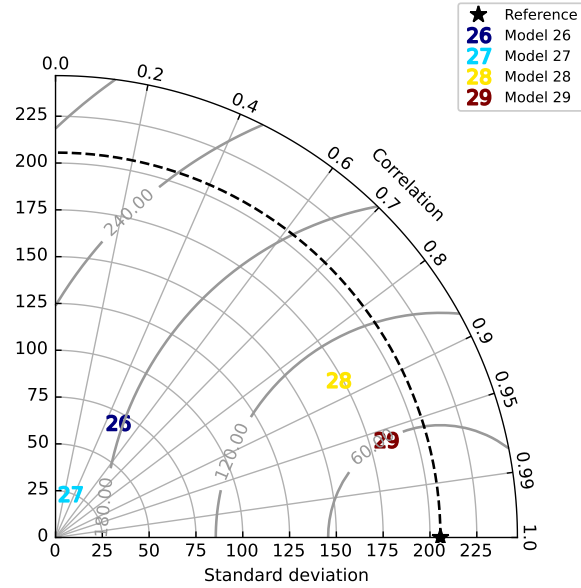


Figure 8: The Taylor diagram of the implicit ML-driven models where Model 26 - NN; Model 27 - ANFIS; Model 28 - ElasticNet; Model 29 - SVM.

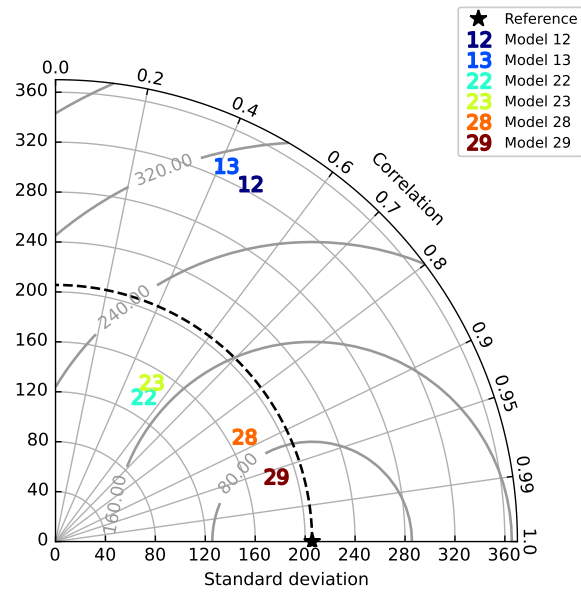


Figure 9: The Taylor diagram of the state-of-art models in each branches where Model 12 - Zeng and Huai / 2014; Model 13 - Disley et al. / 2014; Model 22, 23 - Memarzadeh R., et al.; Model 28 - ElasticNet; Model 29 - SVM.

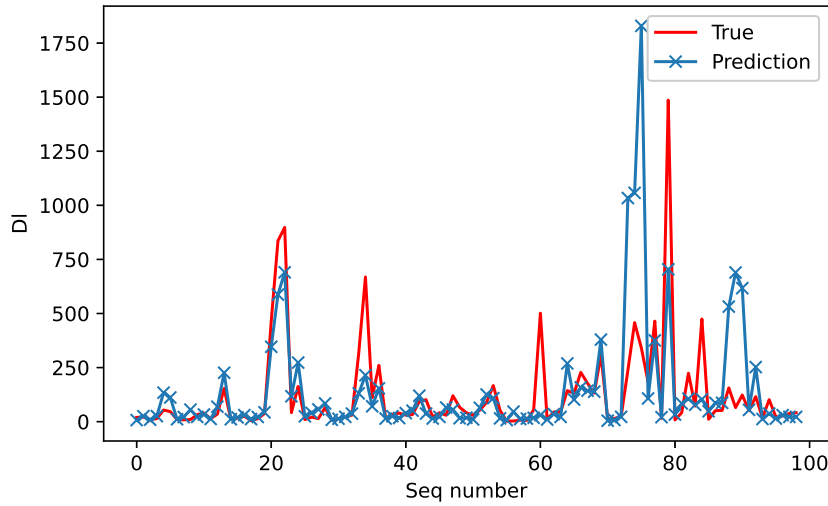


Figure 10: Point to point plot of randomly selected samples

model is developed on 503 samples and this model shows much better prediction and generalization ability than all other symbolic models. Apart from its advantages in the algorithm, a strong data basis is the key to its performance advantage. Moreover, The application range of  $D_l$  prediction models will usually exceed the training dataset. It is difficult to draw effective evaluation conclusions from small datasets. On the contrary, a large dataset can give a more comprehensive result of the model under different circumstances, especially the biased situation. In conclusion, a large and convincing dataset is needed for the regression of the  $D_l$ .

Another factor concerns the characteristics of regression methods themselves. Depending on the regression ability, those regression methods can be split into three levels. The statistical method has weak regression ability and cannot learn many patterns from the data, which leads to poor generalization ability. On the contrary, some implicit ML-driven methods, such as NN have very strong regression ability. However, this advantage didn't bring much improvement in performance. According to the low RMSE value but small R2 of NN in evaluation result compared with model 9 in Table 7, it can be inferred that these methods attempt to learn from the noise instead of physical patterns. In addition, there are not many empirical paradigms on the training of NN and other similar network models, which makes overfitting a common phenomenon. This can lead to problems with good training results but poor testing results. Interestingly, methods with medium regression ability achieve much better results, such as explicit ML-driven methods and simplified implicit ML-driven methods (SVM and ElasticNet). The regression ability of these methods is better than that of statistical methods. But they do not reach the level of depicting the noise, which brings an excellent generalization and extrapolation ability.

## 4 Methods

Evolutionary symbolic regression network (ESRN) proposed in this paper is a novel explicit ML-driven method, which combines the genetic algorithm (GA) and the neural network. The detailed information about these two algorithms are included in the supplementary material, Section S4.

The main idea of this algorithm is to search for the global optimal solution with GA on the basis of local optimal solutions provided by NN. That is because gradient optimization of NN will have its defects on discrete problems, while GA can bridge this problem with its applicability in both discrete and continuous situations. The origin of this idea is from two characteristics of NN:

I. NN can represent many kinds of formulas

With a well defined activation table (Table 9), all kinds of equations can be encapsulated into a network (Fig. 11). The topology and weights of NN will represent the combination and parameters of the equation separately. This makes NN an interpretable symbolic combination and easier to understand.

Table 9: The list of selected activation function

$$\begin{aligned}
 a_1(x) &= 1 \\
 a_2(x) &= x \\
 a_3(x) &= e^x \\
 a_4(x) &= \ln(|x|) \\
 a_5(x) &= \frac{1}{1+e^{-x}}
 \end{aligned}$$

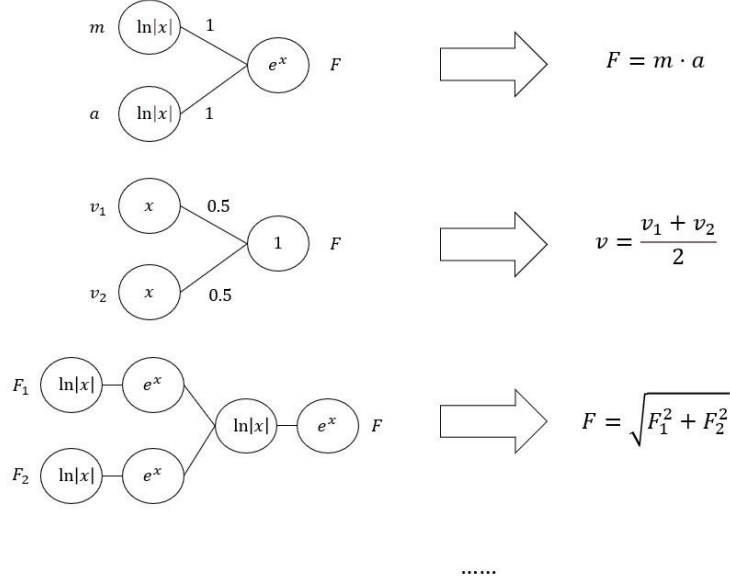


Figure 11: Examples of expressing formulas with NN

## II. A strong regression ability

Universal Approximation Theorem[71] reveals a striking feature of NN: for any distribution, there is always a corresponding network which can learn and imitate its patterns. This makes NN a robust solution for prediction.

The general framework of this evolutionary regression network is listed as follows. For better understanding, A flow chart is provided (Fig. 12).

- (1) The setting of hyper-parameters:  $N$  - the population size;  $M$  - the evaluation metric;  $T$  - the iteration time;  $S_n$  - the topology restriction vector, which limits the number of neurons in each layer. (for example, [3,2,1] stands for a three-layer network, with 3 input neurons, 2 hidden neurons and 1 output neuron in each layer at most)
- (2) Dimensional analysis(DA): Parameters for the  $D_l$  prediction are  $w(m)$ ,  $d(m)$ ,  $U(m/s)$ ,  $U^*(m/s)$ , which have known units. Combined with the unit of those physical quantities, dimensional analysis is carried out to find possible parameter combinations.
- (3) Generation: According to those combinations,  $N$  neural networks with topology according to  $S_n$  will be generated as initial population with random inputs and outputs.
- (4) Training: These candidates will be trained in batch with Adam.
- (5) Evaluation and ranking: Those NNs will be evaluated and ranked according to  $M$ . The first  $N$  networks will be kept and the rest dumped.
- (6) Verification: the iteration time will be checked whether it is lower than  $T$ . If lower, go to 7; otherwise, go to 8.
- (7) Evolution: NNs generated in (3) will serve as the genome for GA evolution. The main evolution process refers to the topology modification of NNs according to mutation and crossover strategies. New candidates will be generated. The main purpose of this step is to expand the solution search space, which is the key to obtaining a global optimal solution. Then go to 3.

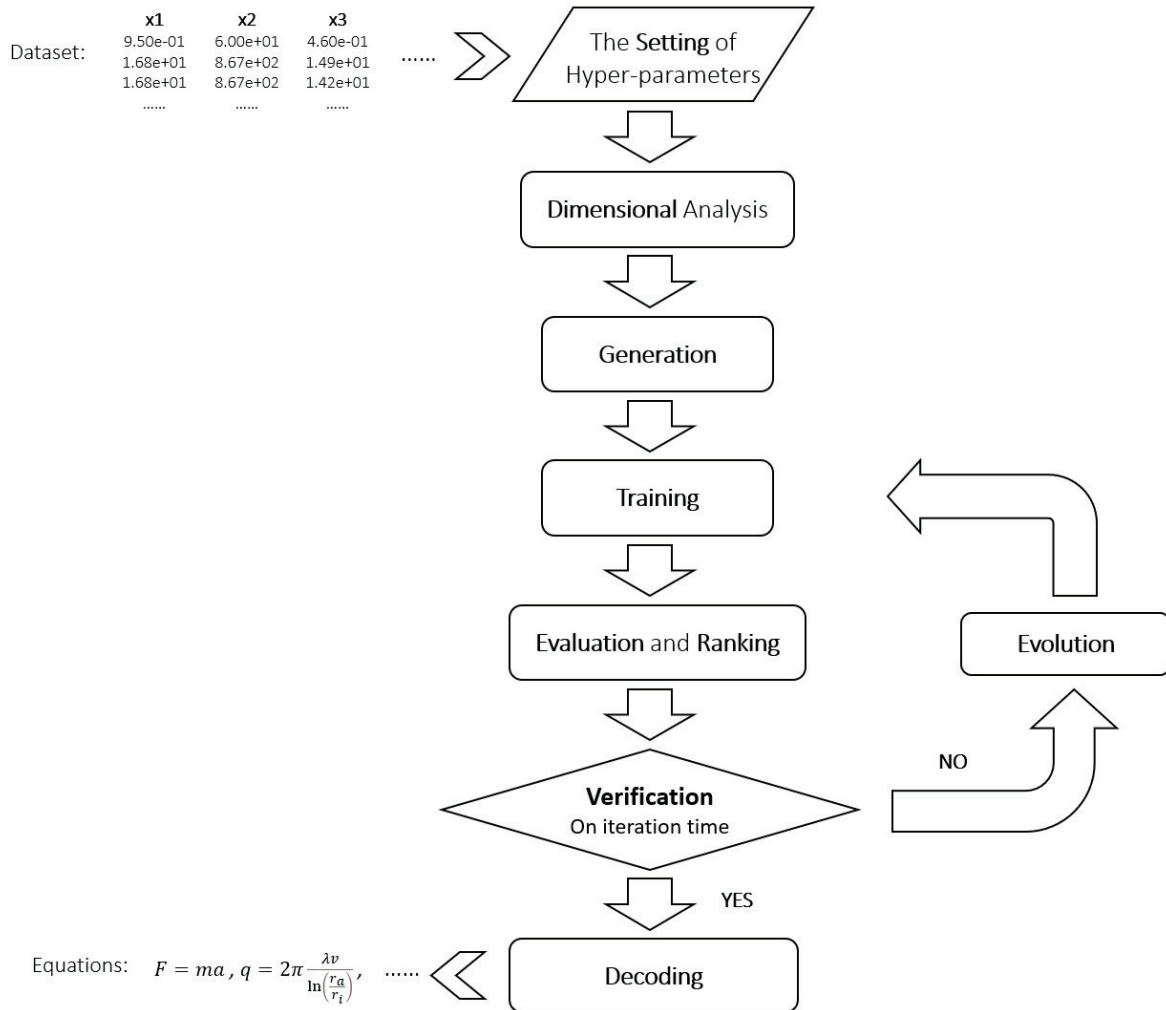


Figure 12: Flow chart of the evolutionary symbolic regression network

(8) Decoding: The top NN will be transferred into a symbolic equation for further analysis.

To illustrate more details, processing on Dimensional Analysis, crossover, mutation and avoidance of overfitting will be explained and discussed.

**Dimensional Analysis:** All physical phenomena can be described by governing equations, which always keep a same dimension at both sides of the formula. This property is called dimensional homogeneity. The homogeneity in dimensions often simplifies the problem and brings advantages to regression. Therefore, parameters from this problem are transferred into a dimensionless combination according to the Buckingham  $\pi$  theorem. The  $\pi$  theorem states that a function of  $n$  variables with  $m$  dimensional units (Eq. 6) can be reorganized as a similar one with  $(n - m)$  dimensionless variables (Eq. 7).

$$y = f(x_1, x_2, \dots, x_n), \text{ with } m \text{ dimensional units} \quad (6)$$

where  $x_i$  = the dimensional input;  $y$  = the dimensional output

$$\pi_y = f(\pi_1, \pi_2, \dots, \pi_{n-m}) \quad (7)$$

where  $\pi_y$  = the dimensionless output;  $\pi_x$  = the dimensionless input



Table 10: Unit table of parameters

Parameter	Unit	L	T
$w, d$	m	1	0
$U, U^*$	m/s	1	-1

Unit matrix  $M_x^u$  is defined as a combination of unit vector  $u_i$  corresponding to the input variable  $x_i$  and unit matrix  $M_y^u$  corresponding to the output variable  $y_i$ .  $N$  and  $p$  are solutions to equation  $M_x^u N = 0$  and  $M_x^u p = M_y^u$ . Then Eq. 6 and Eq. 7 can be connected with the relationship stated in Eq. 8.

$$\pi_{xi} = \prod_{j=1}^n x_j^{N^{ij}},$$

$$\pi_y = \frac{y}{\pi_y^*}, \quad \text{where } \pi_y^* = \prod_{j=1}^n x_j^{p^j} \quad (8)$$

The physical units of variables in this prediction problem are listed in Table 10. Since there are multiple variables with the same unit, the possible combination can be enlarged by replacing  $p$  with a linear combination of  $p$  and  $N$ . Through above operations, the parameter candidates for further analysis are:  $\frac{w}{d}, \frac{U}{U^*}$  and constant 1 for input;  $\frac{D_l}{wU}, \frac{D_l}{wU^*}, \frac{D_l}{dU}, \frac{D_l}{dU^*}$  for output.

The crossover and mutation are the key for this algorithm to evolve expression and find the global optimal solution. Randomness will be utilized in the following parts frequently. It can guarantee a exploration of existing form (4) and other possible combinations in the solution space. The introduce of randomness is designed to bring diversity into the search of expression. Therefore, the specific form of randomness is not important, as long as it can create difference. In this framework, random values with uniform distribution are selected and used in all cases.

**Crossover:** The crossover strategy focuses on finding a better topology combination in the existing group. In ESRN, sub-networks connected to the output neuron will be exchanged randomly between different candidates NNs (Fig. 13). Through generations of selection, better topologies will be obtained and worse discarded.

**Mutation:** Mutation is a more radical strategy. It can enlarge the solution search space and bring unexpected results. Two modes are utilized here, which are activation mutation and candidate mutation.

Activation mutation (Fig. 14) refers to stochastic modification of the activation function in neurons. It can bring a new combination of equations into the system. All neurons in the network are able to have this mutation. Both original and mutated networks will be kept in the population.

Candidate mutation (Fig. 15) refers to a random change of input and output dimensionless candidates mentioned in dimensional analysis. It will adjust those dimensionless combinations randomly within each branches and enable the algorithm to explore more input-output options. The processing strategy is the same as the activation mutation. Both origin and the mutation will both be kept.

**Avoidance of overfitting:** As mentioned, overfitting is a frequent problem in existing studies. It can degrade the generalization ability of the model severely. To avoid overfitting, it is crucial to acquire the performance of a model on both training and testing sets. Therefore, a  $R^2$ -generation plot will be proposed. This plot is a visualization of the top model's  $R^2$  in each generation and the generation time during training and testing. It can reveal the trend of the model's generalization performance. Through artificial selection based on the trend, the optimal model can be obtained. The reason for adopting  $R^2$  as the evaluated metric is the common existence of extreme predictions (Fig. 10). Other metrics such as MSE are sensitive to those extreme values and cannot fully reflect the performance of the model. On the contrary,  $R^2$  is a normalized measure, which can consider the difference not only between true and predictive values but also predictions and their average. It is less affected by those extreme values.

## 5 Results and evaluations

Hyper-parameters used in this experiment are listed in Table 11.

The  $R^2$ -generation plot during the implementation of ESRN is shown in Fig. 16. It is clear that  $R^2$  of the training set keeps rising with the increase of generation, while  $R^2$  of the testing set first increases and then decreases. It reaches the

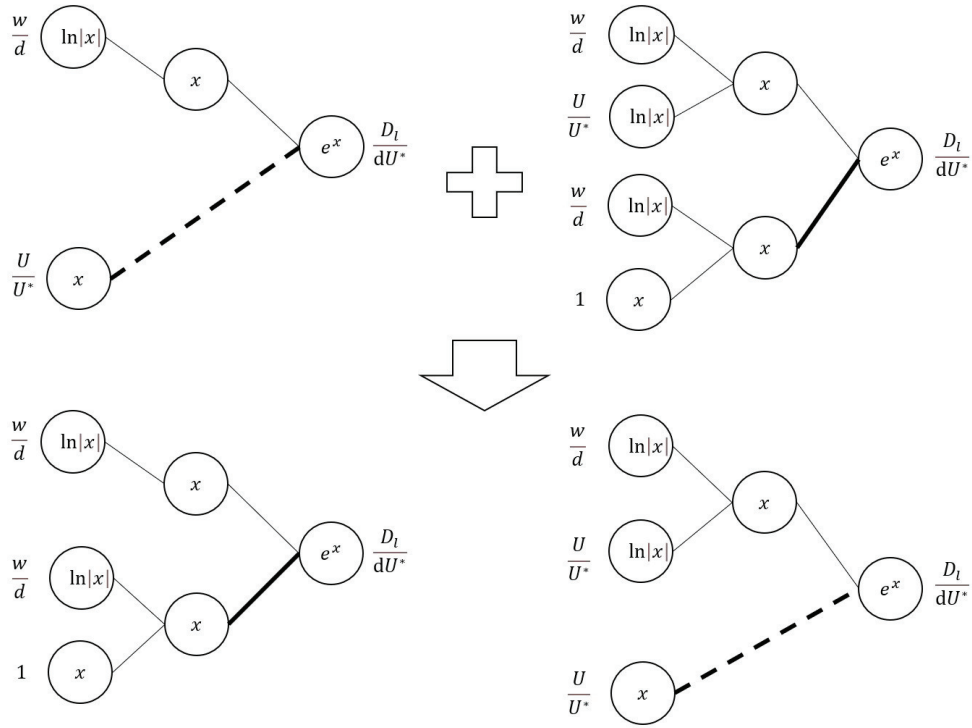


Figure 13: The crossover strategy

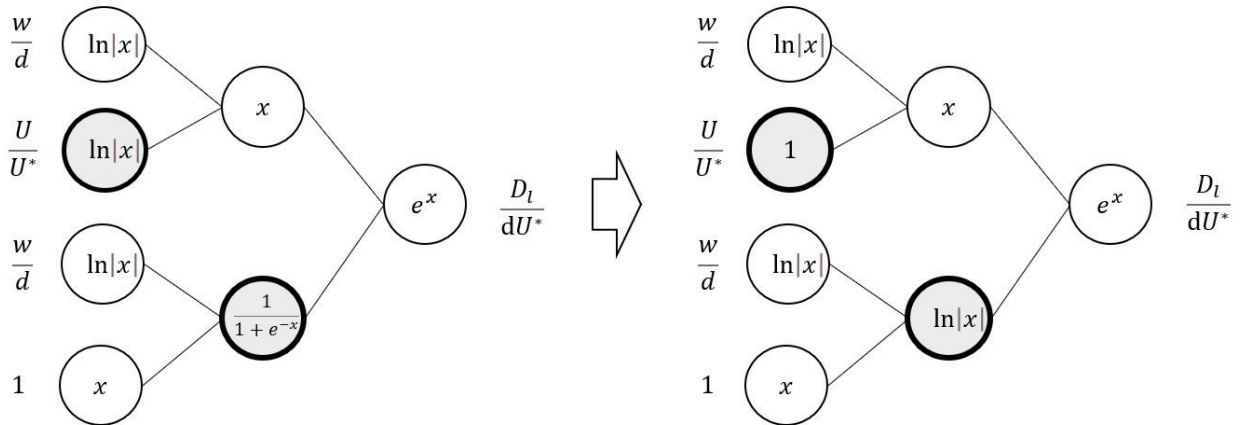


Figure 14: The activation mutation

Table 11: The table of hyper-parameters

$N$	$S_n$	$T$	$M$
100	[5,3,1]	200	$R^2$

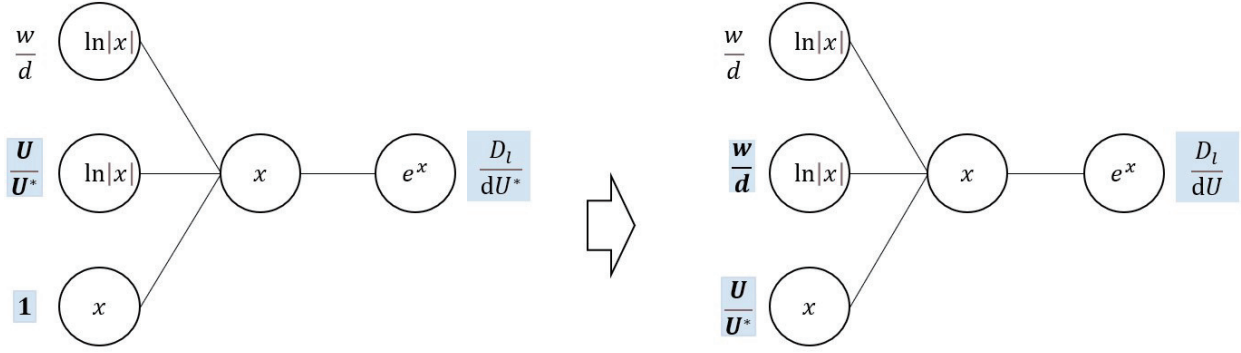


Figure 15: The candidate mutation

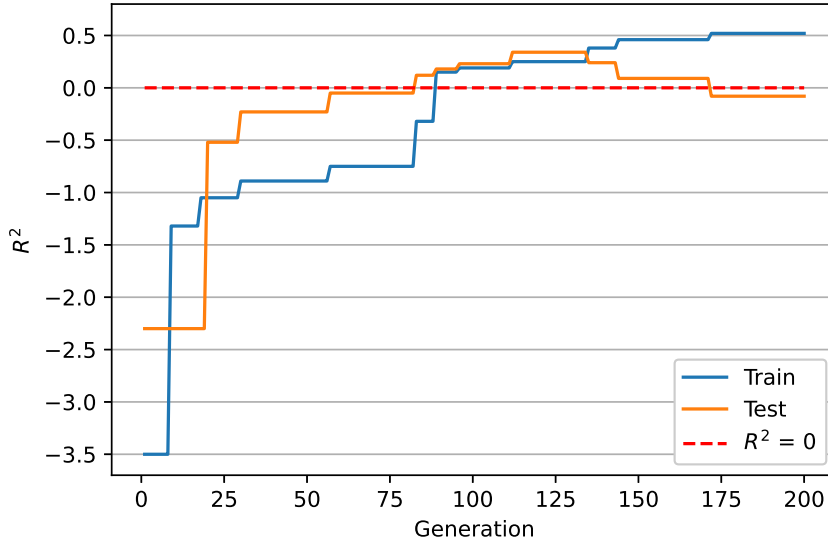


Figure 16: The  $R^2$ -generation plot during the implementation of ESRN

peak value from 112 to 135 generation. This reveals that top models after 135 generation are overfitting and the best model locates between 112 to 135 generation.

The model distilled by ESRN during 112 to 135 generations is very elegant. The optimal network topology is shown in Fig. 17. Basically, it shares a similar topology with previous studies (Eq. 4). The corresponding equation converted from the topology is shown in Eq. 11.

$$\frac{D_l}{dU} = e^{1 \times \ln|\frac{w}{d}| - 1 \times \ln|\frac{U}{U^*}| + 1 \times 2.63} \quad (9)$$

$$\frac{D_l}{dU} = e^{2.63} \left(\frac{w}{d}\right)^1 \left(\frac{U}{U^*}\right)^{-1} \quad (10)$$

$$D_l = 13.89wU^* \quad (11)$$

To evaluate this model, performance metrics, scatter plot of observations and predictions, DR distribution plot and accuracy plot are calculated and implemented on the testing set.

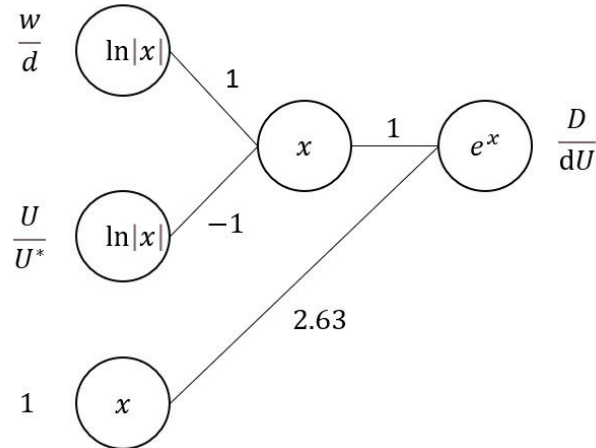


Figure 17: The topology of the result

Table 12: Table of the performance metrics

Model	RMSE	WMAPE	$R^2$
ESRN	32.29	0.52	0.34
$Model_{22}$	38.00	0.58	0.11
$Model_{23}$	38.45	0.59	0.09

The state of art research in explicit ML-driven method, two models of Memarzadeh R., et al. / 2020, are selected for comparison.

The performance metrics of these 3 models on the testing set are listed in Table 12. All Metrics are in reasonable ranges. The errors of two models from [58] are almost the same, which is consistent with the previous comparison in Section 3. The ESRN model shows superiorities in all indexes.

Where  $Model_{22}$  - Memarzadeh R., et al. / 2020;  $Model_{23}$  - Memarzadeh R., et al. / 2020.

Fig. 18 is the scatter plot of true and predicted values from different models. To make the result more intuitive, samples are sorted in ascending order according to the value of D. It can be found that when  $D_l < 25$ , i.e., sequence number less than 125, the three models are similar and all able to reproduce the pattern of true values. When  $25 < D_l < 50$ , i.e. sequence number between 125 to 175, only the ESRN model can provide a more precise estimation.  $Model_{22}$  and  $Model_{23}$  suffer from obvious underestimation. When  $D_l > 50$ , i.e. sequence number over 175, all models underestimate while the prediction of ESRN model is the closest to the true value. This reveals a wider applicability and stability of the ESRN model.

The DR distribution for three models is shown in Fig. 19. For  $Model_{22}$  and  $Model_{23}$ , DR is mainly located in  $DR \leq -0.3$  and  $-0.3 \leq DR \leq 0$ . This reveals that the prediction of  $Model_{22}$  and  $Model_{23}$  is more likely to be lower than the truth. And the main error is underestimation. On the contrary, the ESRN model tends to give slightly larger predictions, which can bring advantages in practical applications. That is because a larger estimation can offer more security redundancy, especially in the prediction of pollution transport.

The accuracy plot reveals that the ESRN model has the highest accuracy (Fig. 20). Although the accuracy gap between the ESRN and  $Model_{22}$  is small, ESRN model has better application potential considering the simplicity and lower demand for parameters.

For more precise evaluation on different research methods, Taylor diagram of representative models from each method and ESRN model is plotted on whole, training and testing dataset. As shown in Fig. 21, the distribution of those models is slightly different on distinct datasets, but the relative positions are in consistency. The overall performance of ESRN locates between model 3 and model 5, which means it has surpassed the state of art explicit ML-driven research with a much simpler form. It is clear that the ESRN model is now the superior symbolic model in the estimation of  $D_l$ . Although there is still a gap between ESRN and implicit models, its conciseness and explicability are enough to make up for this shortcoming. However, implicit ML-driven methods, model 28 and 29, still perform better due to their advantage in model complexity.

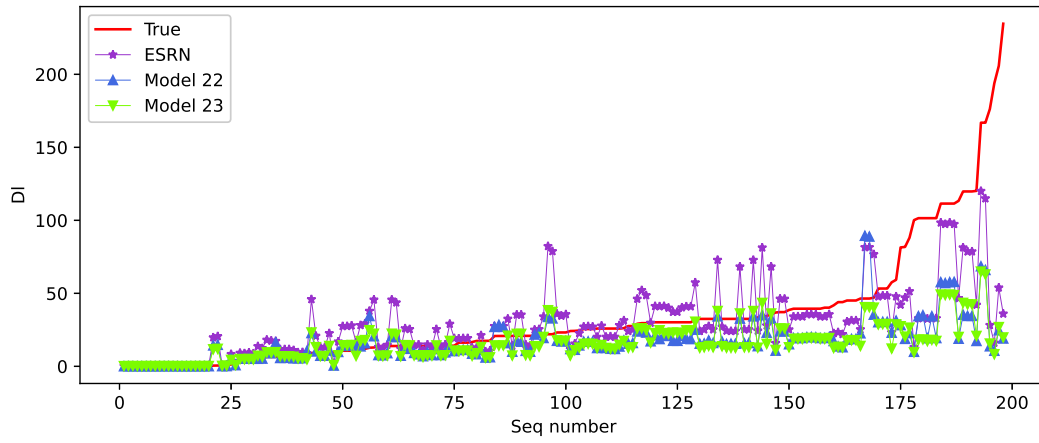


Figure 18: The scatter plot of true and predicted values

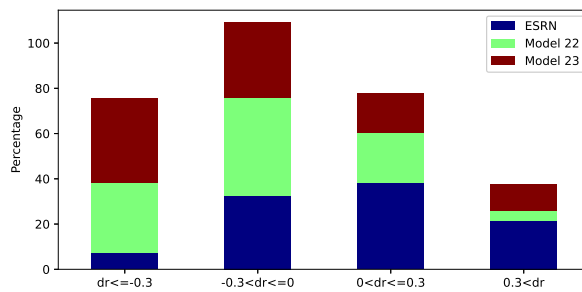


Figure 19: The DR distribution plot

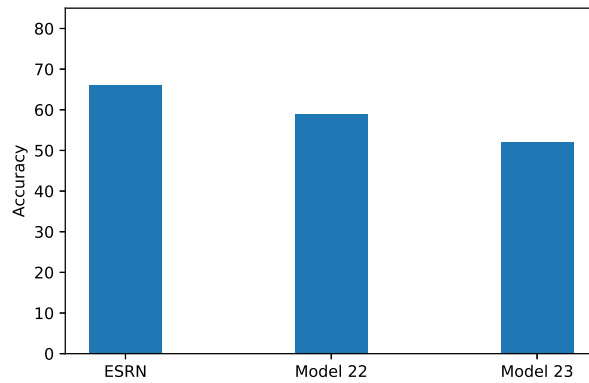
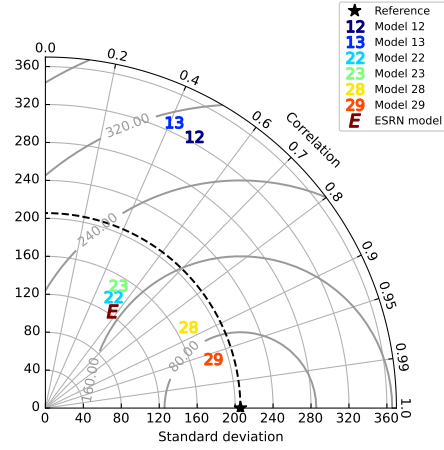
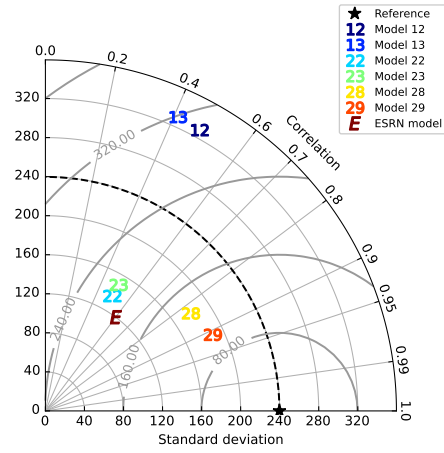


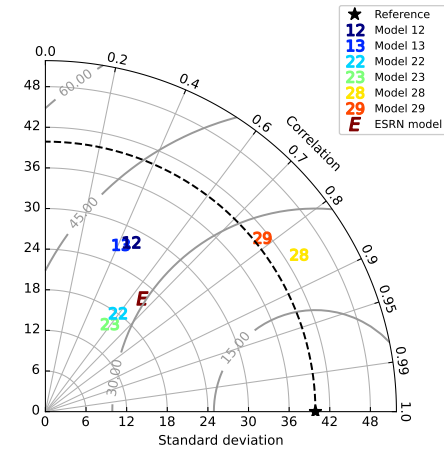
Figure 20: The accuracy plot



(a) Whole dataset



(b) Training dataset



(c) Testing dataset

Figure 21: The visual comparison of the ESRN model with other state-of-art models in each method-branches on whole, training and testing dataset where Model 12 - Zeng and Huai / 2014; Model 13 - Disley et al. / 2014; Model 22, 23 - Memarzadeh R., et al. / 2020; Model 28 - ElasticNet model; Model 29 - SVM model.

In this equation, only  $w$  and  $U^*$  are involved in the final form. This is reasonable from two aspects: the performance advantage and the variable correlation. The performance advantage is already illustrated above. As for the variable correlation, the SCC plot has to be mentioned (Fig. 4). It can be found that the relationship between  $w$  and  $d(0.78)$  is strong. This indicates that only one of them is already able to express all the information on channel geometrics and both can represent as the characteristic length for the channel. Considering  $w$  has a stronger connection to the  $D$ , it is proper to use only  $w$ . A similar relationship can be found between  $U$  and  $U^*$ . But the situation is more complicated in stream properties. It is worth noting that  $U^*$  has a much weaker relationship with  $w$  and  $d$  than  $U(w - U=0.23, w - U=0.29 > w - U^*=0.07, w - U^*=0.11)$ , which reveals an independence between  $U^*$  and  $w, d$ . Considering the strong connection between  $U$  and  $U^*$ , the importance of  $U^*$  is over  $U$ . Therefore,  $w$  and  $U^*$  in this dataset are the most important variables to prediction of  $D_l$ . A model of only  $w$  and  $U^*$  is reasonable. Moreover, the proposed equation is more consistent with the training data in parameter correlation than other general form formulas (Eq. 4). As shown in Fig. 4, all parameters in the dataset are in positive correlation with  $D_l$ . But Due to the limitation of formula form, this relationship cannot be satisfied in most of other existing equations. Taking Model 7 (Liu et al./1977) for example, it is defined as:

$$D_l = 0.18 \frac{w^2 U^{0.5} (U^*)^{0.5}}{d} \quad (12)$$

It is clear that  $d$  is in negative correlation with  $D_l$ , which violates the parameter relationship in the dataset revealed by the SCC plot. This violation is common in other alternatives, which makes the ESRN model become the most physically robust one of all LDC predictive models.

Additionally, the proposed equation shares similarity with Taylor's work in 1954[19]. Taylor's formula is an analytical result for turbulent circular pipe flow when the proposed equation for natural streams. It is defined as:

$$D_l = 10.0 a u_* \quad (13)$$

where  $a$  - the radius of the pipe;  $u_*$  - the shear velocity for circular pipe flow, equal to  $(\frac{g a S}{2})^{0.5}$ .

The methods used to develop these two equations are worlds apart, yet their forms are astonishingly analogous. In the novel equation,  $w$  and  $U^*$  are used. The  $w$  can analogy  $a$  in theory as the characteristic length scale for the channel. Although the definition of  $U^*$ (Eq. 14) is different from  $u_*$ , they are all used to describe the physical influence of velocity gradient, signaling the strength of the shear stress and its influence on the mixture in the presence of flow eddies.

$$U^* = \sqrt{g R S_e} \quad (14)$$

where  $R$  = the hydraulic radius;  $S_e$  = the slope of the energy grade line.

This principle has been overlooked in many previous studies, probably due to their poor regression strategies and limited datasets. With proper treatment of a large dataset, a good division between testing and training sets, as well as the ESRN method, which explores exhaustively a broad range of functional forms for  $D_l$ , we have connected this principle to our model and recovered the turbulent mixture formula as the underlying mechanism in natural stream dispersion processes.

## 6 Conclusions

In this present study, a simple ML-driven explicit model for the prediction of  $D_l$  is proposed with a novel evolutionary symbolic regression network(ESRN). This equation is distilled from a strong data basis of 660 samples collected worldwide (at least increased by 20% than other research), outliers cleaned through IQR and sets divided by SSMD. Basically, this model shares a similar parameter topology with other existing models (Eq. 11). With the search of the optimal parameter combination and the help of robust regression ability, the ESRN algorithm explores multiple symbolic combinations and obtains a globally optimal model with only two input arguments. Various performance metrics and visualization methods are used for further evaluation. As from the comparison, the ESRN model outperforms other existing models in most statistical indexes.

Although this model still suffers from accuracy loss for  $D_l$  over 100, the statistical analysis on the cleaned, extensive dataset collected worldwide (Table 4) reveals that the median and IQR of the overall dataset are 25.90 and 94.33. This indicates that the ESRN model already has the ability to make precise estimations for  $D_l$  than existing alternatives in most application cases all over the world. The above evaluation also shows that the ESRN model tends to give slightly larger values of  $D_l$  than the real ones, which can bring security into its prediction.

Furthermore, the analytical formula given by the ESRN is simple and represents the fundamental physics of turbulent mixing, a principle that has been overlooked in previous studies due to their poor regression strategies on smaller datasets.

Additionally, the performance advantage also indicates that a larger dataset with better processing and suitable division between training and testing sets can offer a more accurate prediction less prone to overfitting.

With advantages of simpler calculation, lower parameter-demand and higher accuracy, the ESRN model is very suitable for practical engineering problems. It can find its place in applications such as estimation of pollution spills, assessment of groundwater etc. The proposed ESRN algorithm performs outstandingly on this four-variable dataset. If a dataset with more input parameters can be provided, it might be able to find an even better variable combination and provide new prediction formulas with stronger performance. Further enhancement on the dataset is needed.

## Acknowledgement

This work was financially supported by Westlake University and The Belt and Road Special Foundation of the State Key Laboratory of Hydrology-Water Resources and Hydraulic Engineering (2019491511).

We also gratefully acknowledge Prof. Ling Li at Westlake University for his useful comments on the manuscript.

## References

- [1] CNN. *The Russian whistleblower risking it all to expose the scale of an Arctic oil spill catastrophe*. Retrieved 11 July 2020.
- [2] Takeuchi Maria R H, Hasegawa Tatsuya, Hardie Susie M L, McKinley Linda E, and Ishihara Keiichi N. Leadership for management of high-level radioactive waste in japan. *Environmental geotechnics*, 7(2):137–146, 2020.
- [3] Elena Savoia, Michael A. Stoto, Rahul Gupta, Nasandra Wright, and Kasisomayajula Viswanath. Public response to the 2014 chemical spill in west virginia: knowledge, opinions and behaviours. *BMC Public Health*, 15(1):790–790, 2015.
- [4] O. Oguntoké, O.J. Aboderin, and A.M. Bankole. Association of water-borne diseases morbidity pattern and water quality in parts of ibadan city, nigeria. *Tanzania journal of health research*, 11(4):189–195, 2010.
- [5] Donald C. Malins, Bruce B. McCain, Donald W. Brown, Sin Lam. Chan, Mark S. Myers, John T. Landahl, Patty G. Prohaska, Andrew J. Friedman, and Linda D. Rhodes. Chemical pollutants in sediments and diseases of bottom-dwelling fish in puget sound, washington. *Environmental Science & Technology*, 18(9):705–713, 1984.
- [6] Anna Kuczyńska, Grzegorz Jarnuszewski, Marzena Nowakowska, Sarah K. Wexler, Zenon Wiśniowski, Piotr Burczyk, Tadeusz Durkowski, and Małgorzata Woźnicka. Identifying causes of poor water quality in a polish agricultural catchment for designing effective and targeted mitigation measures. *Science of The Total Environment*, 765:144125, 2021.
- [7] Mostafa Ramezani, Roohollah Noori, Farhad Hooshyaripor, Zhiqiang Deng, and Amin Sarang. Numerical modelling-based comparison of longitudinal dispersion coefficient formulas for solute transport in rivers. *Hydrological Sciences Journal-journal Des Sciences Hydrologiques*, 64(7):808–819, 2019.
- [8] G. Blöschl and M. Sivapalan. Scale issues in hydrological modelling: A review. *Hydrological Processes*, 9:251–290, 1995.
- [9] Hugo B. Fischer. *Mixing in Inland and Coastal Waters*. 1979.
- [10] Y. Alosairi, S.M. Al-Salem, and A. Al Ragum. Three-dimensional numerical modelling of transport, fate and distribution of microplastics in the northwestern arabian/persian gulf. *Marine Pollution Bulletin*, 161:111723, 2020.
- [11] Hugo Breed Fischer. Longitudinal dispersion in laboratory and natural streams. 1966.
- [12] R. Noori, A.R. Karbassi, H. Mehdizadeh, M. Vesali-Naseh, and M.S. Sabahi. A framework development for predicting the longitudinal dispersion coefficient in natural streams using an artificial neural network. *Environmental Progress*, 30(3):439–449, 2011.
- [13] Rasoul Memarzadeh, Hossein Ghayoumi Zadeh, Majid Dehghani, Hossien Riahi-Madvar, Akram Seifi, and Seyed Mostafa Mortazavi. A novel equation for longitudinal dispersion coefficient prediction based on the hybrid of ssmd and whale optimization algorithm. *Science of The Total Environment*, 716:137007, 2020.



- [14] Il Won Seo and Tae Sung Cheong. Predicting longitudinal dispersion coefficient in natural streams. *Journal of Hydraulic Engineering*, 124(1):25–32, 1998.
- [15] Zhi-Qiang Deng, Vijay P Singh, and Lars Bengtsson. Longitudinal dispersion coefficient in straight rivers. *Journal of Hydraulic Engineering*, 127(11):919–927, 2001.
- [16] M. J. Alizadeh, A. Shabani, and M. R. Kavianpour. Predicting longitudinal dispersion coefficient using ann with metaheuristic training algorithms. *International Journal of Environmental Science and Technology*, 14(11):2399–2410, 2017.
- [17] Mohamad Javad Alizadeh, Davoud Ahmadyar, and Ali Afghantoloe. Improvement on the existing equations for predicting longitudinal dispersion coefficient. *Water Resources Management*, 31(6):1777–1794, 2017.
- [18] Geoffrey Ingram Taylor. Dispersion of soluble matter in solvent flowing slowly through a tube. *Proceedings of The Royal Society A: Mathematical, Physical and Engineering Sciences*, 219(1137):186–203, 1953.
- [19] Geoffrey Ingram Taylor. The dispersion of matter in turbulent flow through a pipe. *Proceedings of The Royal Society A: Mathematical, Physical and Engineering Sciences*, 223(1155):446–468, 1954.
- [20] J. W. Elder. The dispersion of marked fluid in turbulent shear flow. *Journal of Fluid Mechanics*, 5(4):544–560, 1959.
- [21] Hugo B. Fisher. Dispersion predictions in natural streams. *Journal of the Sanitary Engineering Division*, 94(5):927–944, 1968.
- [22] Raul S. McQuivey and Thomas N. Keefer. Simple method for predicting dispersion in streams. *Journal of the Environmental Engineering Division*, 100(4):997–1011, 1974.
- [23] Henry Liu. Predicting dispersion coefficient of streams. *Journal of the Environmental Engineering Division*, 103(1):59–69, 1977.
- [24] Il Won Seo and Tae Sung Cheong. Predicting longitudinal dispersion coefficient in natural streams. *Journal of Hydraulic Engineering*, 124(1):25–32, 1998.
- [25] Antonis D. Koussis and José Rodríguez-Mirasol. Hydraulic estimation of dispersion coefficient for streams. *Journal of Hydraulic Engineering*, 124(3):317–320, 1998.
- [26] Zhi-Qiang Deng, Vijay P Singh, and Lars Bengtsson. Longitudinal dispersion coefficient in straight rivers. *Journal of Hydraulic Engineering*, 127(11):919–927, 2001.
- [27] S. M. Kashfipour and Roger Alexander Falconer. Longitudinal dispersion coefficients in natural channels. *Water Research*, 36(6):1596–1608, 2002.
- [28] Yuhong Zeng and Wenxin Huai. Estimation of longitudinal dispersion coefficient in rivers. *Journal of Hydro-environment Research*, 8(1):2–8, 2014.
- [29] T. Disley, B. Gharabaghi, A. A. Mahboubi, and E. A. McBean. Predictive equation for longitudinal dispersion coefficient. *Hydrological Processes*, 29(2):161–172, 2015.
- [30] Alex Waibel, Toshiyuki Hanazawa, Geoffrey E. Hinton, Kiyohiro Shikano, and Kevin J. Lang. Phoneme recognition: neural networks vs. hidden markov models. In *ICASSP*, pages 107–110, 1988.
- [31] Andrew J. Myles, Alan F. Murray, A. Robin Wallace, John Barnard, and Gordon Smith. Estimating mlp generalisation ability without a test set using fast, approximate leave-one-out cross-validation. *Neural Computing and Applications*, 5(3):134–151, 1997.
- [32] D. L. Toulson, J. F. Boyce, and C. Hinton. Data representation and generalisation in an application of a feed-forward neural net. pages 27–40, 1992.
- [33] P. A. Aguilera, A. Fernández, R. Fernández, R. Rumí, and A. Salmerón. Review: Bayesian networks in environmental modelling. *Environmental Modelling and Software*, 26(12):1376–1388, 2011.
- [34] Francesco Granata, Stefano Papirio, Giovanni Esposito, Rudy Gargano, and Giovanni de Marinis. Machine learning algorithms for the forecasting of wastewater quality indicators. *Water*, 9(2):105, 2017.
- [35] Maruti Kumar Mudunuru and Satish Karra. Physics-informed machine learning models for predicting the progress of reactive-mixing. *Computer Methods in Applied Mechanics and Engineering*, 374:113560, 2021.
- [36] Gokmen Tayfur and Vijay P. Singh. Predicting longitudinal dispersion coefficient in natural streams by artificial neural network. *Journal of Hydraulic Engineering*, 131(11):991–1000, 2005.
- [37] Z. Fuat Toprak and Hikmet Kerem Cigizoglu. Predicting longitudinal dispersion coefficient in natural streams by artificial intelligence methods. *Hydrological Processes*, 22(20):4106–4129, 2008.

- [38] Roohollah Noori, Abdulreza Karbassi, Ashkan Farokhnia, and Majid Dehghani. Predicting the longitudinal dispersion coefficient using support vector machine and adaptive neuro-fuzzy inference system techniques. *Environmental Engineering Science*, 26(10):1503–1510, 2009.
- [39] Hossien Riahi-Madvar, Seyed Ali Ayyoubzadeh, Ehsan Khadangi, and Mohammad Mehdi Ebadzadeh. An expert system for predicting longitudinal dispersion coefficient in natural streams by using anfis. *Expert Systems With Applications*, 36(4):8589–8596, 2009.
- [40] H. Md. Azamathulla and Fu-Chun Wu. Support vector machine approach for longitudinal dispersion coefficients in natural streams. *Applied Soft Computing*, 11(2):2902–2905, 2011.
- [41] Akram Seifi and Hossien Riahi-Madvar. Improving one-dimensional pollution dispersion modeling in rivers using anfis and ann-based ga optimized models. *Environmental Science and Pollution Research*, 26(1):867–885, 2019.
- [42] Behzad Ghiasi, Hossein Sheikhan, Amin Zeynolabedin, and Mohammad Hossein Niksokhan. Granular computing–neural network model for prediction of longitudinal dispersion coefficients in rivers. *Water Science and Technology*, 80(10):1880–1892, 2019.
- [43] Rajeev Ranjan Sahay and Som Dutta. Prediction of longitudinal dispersion coefficients in natural rivers using genetic algorithm. *Hydrology Research*, 40(6):544–552, 2009.
- [44] Amir Etemad-Shahidi and Milad Taghipour. Predicting longitudinal dispersion coefficient in natural streams using m5' model tree. *Journal of Hydraulic Engineering*, 138(6):542–554, 2012.
- [45] Xiangtao Li, Huawen Liu, and Minghao Yin. Differential evolution for prediction of longitudinal dispersion coefficients in natural streams. *Water Resources Management*, 27(15):5245–5260, 2013.
- [46] Ahmed M.A. Sattar and Bahram Gharabaghi. Gene expression models for prediction of longitudinal dispersion coefficient in streams. *Journal of Hydrology*, 524:587–596, 2015.
- [47] Yufei Wang and Wenxin Huai. Estimating the longitudinal dispersion coefficient in straight natural rivers. *Journal of Hydraulic Engineering*, 142(11):4016048, 2016.
- [48] Yu-Fei Wang, Wen-Xin Huai, and Wei-Jie Wang. Physically sound formula for longitudinal dispersion coefficients of natural rivers. *Journal of Hydrology*, 544:511–523, 2017.
- [49] Hossien Riahi-Madvar, Majid Dehghani, Akram Seifi, and Vijay P. Singh. Pareto optimal multigene genetic programming for prediction of longitudinal dispersion coefficient. *Water Resources Management*, 33(3):905–921, 2019.
- [50] Hossien Riahi Madvar, Majid Dehghani, Rasoul Memarzadeh, Ely Salwana, and Amirhosein Mosavi. Derivation of optimized equations for estimation of dispersion coefficient in natural streams using hybridized ann with pso and cso algorithms. *IEEE Access*, 8:156582–156599, 2020.
- [51] Erhard Rahm and Hong Hai Do. Data cleaning: Problems and current approaches. *IEEE Data(base) Engineering Bulletin*, 23:3–13, 2000.
- [52] S. M. Kashefipour and Roger Alexander Falconer. Longitudinal dispersion coefficients in natural channels. *Water Research*, 36(6):1596–1608, 2002.
- [53] Gokmen Tayfur and Vijay P. Singh. Predicting longitudinal dispersion coefficient in natural streams by artificial neural network. *Journal of Hydraulic Engineering*, 131(11):991–1000, 2005.
- [54] Meredith L. Carr and Chris R. Rehmann. Measuring the dispersion coefficient with acoustic doppler current profilers. *Journal of Hydraulic Engineering*, 133(8):977–982, 2007.
- [55] Z. Fuat Toprak and Hikmet Kerem Cigizoglu. Predicting longitudinal dispersion coefficient in natural streams by artificial intelligence methods. *Hydrological Processes*, 22(20):4106–4129, 2008.
- [56] Roohollah Noori, Abdulreza Karbassi, Ashkan Farokhnia, and Majid Dehghani. Predicting the longitudinal dispersion coefficient using support vector machine and adaptive neuro-fuzzy inference system techniques. *Environmental Engineering Science*, 26(10):1503–1510, 2009.
- [57] Amir Etemad-Shahidi and Milad Taghipour. Predicting longitudinal dispersion coefficient in natural streams using m5' model tree. *Journal of Hydraulic Engineering*, 138(6):542–554, 2012.
- [58] Rasoul Memarzadeh, Hossein Ghayoumi Zadeh, Majid Dehghani, Hossien Riahi-Madvar, Akram Seifi, and Seyed Mostafa Mortazavi. A novel equation for longitudinal dispersion coefficient prediction based on the hybrid of ssmd and whale optimization algorithm. *Science of The Total Environment*, 716:137007, 2020.
- [59] Rajeev Ranjan Sahay. Prediction of longitudinal dispersion coefficients in natural rivers using artificial neural network. *Environmental Fluid Mechanics*, 11(3):247–261, 2011.

- [60] David J Hand and Niall M Adams. Data mining. *Wiley StatsRef: Statistics Reference Online*, pages 1–7, 2014.
- [61] Alan J. Miller. *Subset Selection in Regression*. 2002.
- [62] Björn Barz and Joachim Denzler. Do we train on test data? purging cifar of near-duplicates. *Journal of Imaging*, 6(6):41, 2020.
- [63] R. W. Kennard and L. A. Stone. Computer aided design of experiments. *Technometrics*, 11(1):137–148, 1969.
- [64] David R. Roberts, Volker Bahn, Simone Ciuti, Mark S. Boyce, Jane Elith, Gurutzeta Guillera-Arroita, Severin Hauenstein, José J. Lahoz-Monfort, Boris Schröder, Wilfried Thuiller, David I. Warton, Brendan A. Wintle, Florian Hartig, and Carsten F. Dormann. Cross-validation strategies for data with temporal, spatial, hierarchical, or phylogenetic structure. *Ecography*, 40(8):913–929, 2017.
- [65] Christopher M. Bishop. *Pattern Recognition and Machine Learning*. 2006.
- [66] Simon Haykin. *Neural Networks: A Comprehensive Foundation*. 1998.
- [67] Kurata Gakuto. Method to leverage similarity and hierarchy of documents in nn training, 2019.
- [68] David E. Goldberg. *Genetic algorithms in search, optimization, and machine learning*. 1989.
- [69] Stephen Boyd and Lieven Vandenberghe. *Convex Optimization*. 2004.
- [70] Jorge Nocedal and Stephen J. Wright. *Numerical Optimization*. 2006.
- [71] K. Hornik, M. Stinchcombe, and H. White. Multilayer feedforward networks are universal approximators. *Neural Networks*, 2(5):359–366, 1989.